AIR FORCE INSTITUTE OF TECHNOLOGY

AIR UNIVERSITY
UNITED STATES AIR FORCE

EFFECT OF FLAP BLOWING ON THE SECTIONAL CHARACTERISTICS OF AN NACA 0015 AIRFOIL

THESIS

GAM 65A/AE/65-2

Rayford P. Patrick
1/Lt USAF

SCHOOL OF ENGINEERING

WRIGHT-PATTERSON AIR FORCE BASE, OHIO

EFFECT OF FLAP BLOWING ON THE SECTIONAL

CHARACTERISTICS OF AN NACA 0015 AIRFOIL

THESIS

Presented to the Faculty of the School of Engineering of

the Air Force Institute of Technology

Air University

in Partial Fulfillment of the

Requirements for the Degree of

Master of Science

by

Rayford P. Patrick, B.S.A.E.

1/Lt USAF

Graduate Aerospace Mechanical Engineering

March 1965

Preface

In this report is presented the results of a wind-tunnel study conducted in the AFIT Five-Foot Wind Tunnel. It is hoped that the results presented in this report might aid in the choice of landing and take-off configurations of today's modern, high-speed aircraft.

I would like to express appreciation to my advisor, Professor H. C. Larsen for his timely assistance, to the wind-tunnel technicians, W. S. Whitt and Al Barringer for their aid, and my family for their endurance.

Rayford P. Patrick

Contents

List of Figures

Figure | Page

List of Tables

List of Symbols

c	Chord length of the model, inches
C.P.	Pressure coefficient
$C.P._L$	Pressure coefficient on lower surface of the model
$C.P._u$	Pressure coefficient on upper surface of the model
C_D	Sectional profile drag coefficient
C_{D_P}	Sectional pressure drag coefficient
C_H	Sectional hinge moment coefficient
C_L	Sectional lift coefficient
C_{Lmax}	Maximum sectional lift coefficient
C_{mle}	Moment coefficient about the leading edge of the model
C_μ	Momentum or blowing coefficient
$C_{\mu crit}$	Moment coefficient required to obtain theoretical flap effectiveness
g	Gravitational constant, lb_m ft/lb_f sec^2
$\dot{m}$	Mass-flow rate of blowing air, lb_m/sec
P	Local static pressure, lb_f/ft
P_1'	Static pressure at the entrance to the orifice plate of the flowmeter, psia
P_e	Static pressure of the exit of the blowing slot, psia
P_o	Total pressure in the plenum chamber of the flap, psia
P_∞	Free-stream static pressure, lb_f/ft^2
q	Local dynamic pressure, lb_f/ft^2
q_o	Free-stream dynamic pressure
R	Gas constant for air, $\frac{lbf\ ft}{lb_m\ {}^\circ R}$
S	Model wing area, ft^2
T_e	Temperature of the blowing air, °R

V_e Velocity at the exit of the blowing slot, ft/sec

$\Delta P'$ Change in static pressure across the orifice plate of the flowmeter, in Hg

α Angle of attack of the model, degrees

γ Ratio of specific heats

δ_F Flap deflection of the model, degrees

Abstract

The purpose of this investigation was to determine the effect on the sectional characteristics of an NACA 0015 airfoil section of blowing over the leading edge of the trailing-edge flap.

Results of this investigation showed that C_L, C_H, C_{mle}, and C_{Lmax} increased with C_μ, while C_{D_p} decreased, the optimum S_F for maximum increase in C_L was 45° at a C_μ of .039, and the optimum S_F for maximum increase in C_L per C_μ was 30° at a C_μ of .028. The data-reduction computer program is included in Appendix B.

EFFECT OF FLAP BLOWING ON THE SECTIONAL CHARACTERISTICS OF AN NACA 0015 AIRFOIL

I. Introduction

Background

History. Near the end of the nineteenth century, fluid mechanics began to develop into two separate branches. One branch was theoretical and the other was largely empirical. The theoretical branch dealt with the equations of motion for an inivisid, ideal fluid. The empirical branch, hydralics, developed because theory failed to describe real fluid flow. Using experimental data and curve fitting techniques, engineers developed empirical equations that described certain flows quite well.

At the beginning of the twentieth century, Prandtl made a significant contribution. He realized that the reason theory disagreed with experiment was that the ideal fluid theory neglected the viscous effects of the fluid. Viscous forces seemed to be very small when compared to the pressure and inertial forces of a flow with a large Reynold's Number and hence were neglected. Prandtl, though, showed that, in a small region of flow near a solid boundary, viscous forces are of the same order of magnitude as the inertial forces and must be considered. He called this region the boundary layer. The region of flow outside the boundary layer could be accurately characterized by the ideal fluid equations, which neglected viscous effects. This boundary layer concept proved to be the basis of real fluid mechanics.

The velocity of the fluid in continuum flow in the boundary layer ranges from near zero at the boundary to the free-stream value at the edge of the boundary layer. Therefore, the particles of fluid in the boundary layer have lower velocities than the free stream and consequently lower energy. These low-energy particles do not always remain adjacent to the boundary, if the wall is curved. This curvature induces an unfavorable pressure gradient which causes a flow reversal in the boundary layer. This flow reversal causes the boundary layer to be forced away from the boundary, or to be separated. Downstream of a body, whose boundary layer has separated, there exists a region of low-energy flow (the separated boundary layer). This region causes an enormous increase in drag and a decrease in lift.

Because of these adverse effects, several methods have been developed to delay separation. Ejection of high-energy air into the boundary layer, suction of low-energy from the boundary layer, and prevention of separation by use of suitable airfoil configurations (slots, slats, etc.) are the most common methods in use today.

All of the above methods greatly improve the low-speed characteristics of an airfoil. However, the actual changing of an airfoil's geometry gives rise to aerodynamical problems at higher velocities. On the other hand, blowing and suction do not change the shape of an airfoil and may be used with any airfoil. Since the advent of the jet engine, blowing has become the most advantageous form of boundary layer control because of the large mass rate of flow of air through the engine. Some of this air can be bled off to blow the airfoil with relatively low loss in engine efficiency. On the other hand, suction requires use of additional equipment which increases the weight of the aircraft, partially offsetting the benefit gained by boundary layer control.

Development and Application. Prandtl performed some experiments in boundary layer control in the early twentieth century, but it was not until the 1920's that the other scientists in England, France, Germany, and the United States began conducting experiments in this field. Until the advent of the jet engine in the 1940's, the equipment required for blowing was so heavy, complicated, bulky, and power consuming that no practical application was feasible. The emergence of the jet engine aided the solution of the problem and blowing is now used on many high-speed aircraft for landing and take-off.

Purpose

Aircraft today are either designed for extremely high-speed flight or for highly-maneurvable, low-speed flight. The blowing flap can assist greatly in either design. For the high-speed aircraft, blowing can improve landing, take-off, and low sub-sonic performances greatly. For the low-speed aircraft, blowing can be used to advantage throughout the entire flight.

The purpose of this report is to show the effect of blowing on the characteristics of an NACA 0015 airfoil. Variation of the maximun lift coefficient, the pressure drag coefficient, leading edge and hinge moment coefficients, angle of attack at stall, and slope of lift curves with different momentum coefficients, C_μ, are investigated. The friction drag is investigated and compared to the pressure drag. Also, $C_{\mu crit}$ at several flap deflections, an optimum flap deflection for largest increase in lift, and an optimum flap deflection for largest percentage increase in lift are investigated.

Scope

The test was conducted in the AFIT, Five-Foot Wind Tunnel at a dynamic pressure, q_o, equivalent to two inches of water and a Reynold's Number of 1.2×10^6. The low q_o was necessary to prevent overflow of the manometers at high pressure coefficients. Even at this low q_o, the Reynold's Number was fairly large because of the large model. The tests were at flap deflections of 0, 15, 30, 45, and 60 degrees. C_μ's ranged from .0023 to .147, with the larger C_μ's at higher flap deflections. The angle of attack varied from zero to stall by increments of two degrees, except near stall where increments of one degree were made. There were no negative angle of attack data taken because of the limitations on the set-up. The hose connection between the flap and the external air supply prohibited rotation below an angle of attack of zero.

II. Description of Apparatus

Wind Tunnel

The model was tested in the AFIT, Five-Foot Wind Tunnel, which has a maximum flow speed of 300 miles per hour. The five-foot diameter, circular test section was converted to a two-dimensional section by the installation of large plyboard panels along both sides. The trailing edges of these panels were hinged and attached to servos. There were four pitot-static tubes, mounted on top, bottom, right side and left side of the entrance to the test section. These tubes measured the local q, which is proportional to the velocity squared. The trailing edge flaps were adjusted until the local q's are equal, insuring more uniform flow through the test section.

Airfoil Model

The model used in this investigation was designed by Professor H. C. Larsen, Head of the Aeronautical Engineering Department, and constructed in the AFIT machine shop. The thirty-inch-chord model is an NACA 0015 airfoil with symmetrical flap hinged at 75 percent chord on the center line of the airfoil.

The model has large, sharp-edged, aluminum side-plates which, when mounted in the test section, were one inch from the tunnel two-dimensional section (Fig. 1). These side-plates stripped off the boundary layer which had built up on the tunnel walls and aided in producing a more-nearly, two-dimensional flow over the airfoil.

A total of 71 pressure taps were located on the surface of the airfoil and in the plenum chamber of the flap, of which only 66 pressure taps on the airfoil and the plenum chamber tap were connected because of space limitation. The taps on the surface of the airfoil include a tap at the leading edge of the airfoil, one on the trailing edge, and six on the leading edge of the flap, ten degrees apart. Table I gives the location of the taps.

The slot width, through which the high velocity air was ejected, is located at 75 percent chord. The slot width varied at different flap settings because of slight, off-center rotation of the flap about the hinge line. The effective slot widths at different flap deflections are given in Table II.

Flowmeter

The requirement for accurate measurement of the mass-flow rate $\dot{m}$ of air blown over the flap led to the design, construction, and calibration of a flowmeter. The type chosen was a one inch diameter flowmeter with a .75 inch square-edged orifice in the orifice plate. The flowmeter was calibrated against a standard ASME flowmeter to an accuracy of five percent. Fig. 6 gives the calibration curve of the flowmeter.

Rake

A total-head survey rake was installed nearly two chord lengths downstream of the model. This rake, shown in Fig. 2, has 115 total-head tubes and six static-pressure tubes of which 94 total head tubes and six static-pressure tubes were connected because of the limited number of manometers available.

Manometers

There were two, 100-tube, banks of manometers used for pressure measurement. The pressure taps on the airfoil were connected to a

96-inch-tall bank of vertical manometers filled with alcohol. The rake was connected to a 30-inch bank of manometers inclined 63.5 degrees from the vertical and filled with oil. This inclination allowed small pressure changes to be interpreted more easily and accurately. (Since all calculations were in terms of dimensionless ratios, differences in fluid or in inclination posed no problem.)

Traversing Mechanisms

Because the tunnel two-dimensional section was not equipped for proper mounting and positioning of the model, traversing mechanisms were designed and constructed to permit up and down, and front and back displacement of the model. The model could then be positioned in the exact center of the tunnel, perpendicular to the air stream. Otherwise, with so large a model, there would be a lifting force on the model due to blockage. Fig. 4 shows the completed mechanism (right side) mounted on the two-dimensional section.

Angle of Attack Drive Mechanism

The method used for varing the angle of attack of the model was to attach cables to the fore and aft parts of the side-plate, run the cables down through the floor of the tunnel, and connect them to a motor-driven gear box. A revolution counter attached to the motor was calibrated to an accuracy of ten minutes of arc. Fig. 3 shows the motor, gear box, cables running to model, and the counter cable attached to the electric motor.

Manifold

The blowing air input to the plenum chamber of the flap was located between the side-board of the model and the tunnel two-dimensional section. Because there was only one inch clearence between the two, a manifold was designed and constructed to connect the input receptacle to the high pressure hose from the air supply.

III. Procedure

Before testing proper could begin, there were many preliminary checks and tests to be accomplished. Next, the model and all associated equipment was installed and checked for leakages and/or misalignment. The blowing apparatus was then connected and checked for leaks and dependability.

Physical Set-up

The airfoil and rake were mounted in the tunnel as shown in Figs. 1 and 3 and connected via tubing to the manometer boards. Because of the great amount of data points per run, cameras were set up to take pictures of the manometer boards during each run. The pictures could then be interpreted at some later, more convenient, time. The flowmeter was connected between the air source and the plenum chamber of the flap with standard pressure and temperature measuring apparatus.

Determination of Parameters

Mass-Flow Rate. The mass-flow rates were determined by use of the calibration curve of the flowmeter (Fig. 6). For a particular value of $P_1'\Delta P'$ there is a corresponding mass-flow rate.

Jet Velocity. Because the slot was essentially a convergent nozzle, the air was assumed to expand isentropically from the plenum-chamber total pressure to the static pressure at the exit of the slot. The equation

$$V_e = \left[2gRT_e\left(\frac{\gamma}{\gamma-1}\right) \left\{1 - \frac{P_e}{P_o}\right\}^{\frac{\gamma-1}{\gamma}} \right]^{1/2}$$

was used to calculate the jet velocity. The plenum-chamber total pressure P_o was measured by using a mercury-filled manometer and the exit static pressure was determined from the pressure taps on the leading edge of the flap. The temperature between the flowmeter and the plenum chamber was determined by Lt. Ketter (Ref 4:5) to be constant. Therefore the temperature measured at the flowmeter was used in the jet-velocity calculations.

<u>Momentum Coefficient C_μ</u>. The parameter used in the study of flap blowing was first introduced by Poisson-Quinton (Ref 2:463) and is defined as

$$C_\mu = \frac{\dot{m} V_e}{q_o S} \tag{2}$$

where $\dot{m}$ is the mass-flow rate of the blowing air, V_e is the jet velocity at the slot exit, q_o is the free-stream dynamic pressure and S, in this report, is the chord length (since a two-dimensional airfoil is being considered).

<u>Critical Momentum Coefficient $C_{\mu crit}$</u>. Blowing an airfoil results in two phenomena, boundary layer control at lower values of C_μ, and supercirculation at higher values of C_μ. Initially blowing re-energizes the boundary layer and causes it to reattach to the airfoil, thus giving the realization of flap effectiveness as predicted by potential theory (Ref 2:463). The momentum coefficient required to achieve theoretical flap effectiveness is defined as $C_{\mu crit}$ and can be determined from Fig. 35 for each flap deflection. The slope change on the curves (Fig. 35), from steep slopes (Boundary Layer Control) to gradual slopes (Supercirculation), is designated $C_{\mu crit}$ for each particular flap setting.

Pressure Coefficient C.P. The pressure coefficient is a non-dimensional parameter used in most calculations instead of the static pressure. The primary advantage of the pressure coefficient is that the results obtained are independent of test conditions (i.e., speed, density, absolute pressure, etc.) as long as the effects of Reynold's Number and Mach Number can be neglected. The pressure coefficient is defined as

$$C.P. = \frac{P - P_\infty}{q_o} \tag{3}$$

Lift Coefficient C_L. The life coefficient was determined by an integration of the pressure coefficients around the airfoil. The integration was a numerical one, using the trapezoidal rule and was performed on the IBM 1620 computer according to the equation

$$C_L = \int_0^1 (C.P._L - C.P._u)\, d\left(\frac{x}{c}\right) \tag{4}$$

from Kuethe and Schetzer (Ref 5:218). Appendix B gives the computer program used.

Pressure Drag Coefficient C_{Dp}. Essentially the same type procedure was used to determine C_{Dp} but instead of integrating over a horizontal distance the integration was performed over a vertical distance, i.e., from the geometrical lowest pressure tap to the highest and back to the lowest. This calculation does not include either the induced or the viscous drag.

Drag Coefficient by the Momentum Method. The profile drag coefficient was obtained by comparing the momentum of the air ahead of the model with the momentum behind the model. The loss in momentum between the two sections was equal to the profile drag of the airfoil. An integration over the cross section of the tunnel was accomplished by use of the survey rake and the following equation

$$C_D = \frac{2}{c}\int_0^h \left(\sqrt{\frac{q}{q_o}} - \frac{q}{q_o}\right)dy \tag{5}$$

from Pope (Ref 6:112). This equation was also integrated numerically by the IBM 1620 (Appendix B).

Moment Coefficient C_{mle}. The moment coefficient about the leading edge was determined by calculation of a force at a point on the surface of the airfoil and multiplying by the correct moment arm. The equation used was

$$C_{mle} = -\int_0^1 (C.P._L - C.P._u)\left(\frac{x}{c}\right)d\left(\frac{x}{c}\right) \tag{6}$$

Hinge Moment Coefficient. The hinge moment is the sum of the forces at every point on the flap multiplied by the correct moment arm. The equation is of the same form as Equation (6), where the summation of moments was taken about the hinge line of the flap rather than the leading edge of the airfoil. The same type of numerical integration was used and Appendix B shows the form used in the computer program.

Correction Factors

The conditions under which a model is tested in a wind tunnel are not the same as those in the free atmosphere. There is no appreciable difference because of having the model still and the air moving instead of vice versa. The difference lies in the fact that in a wind tunnel there are solid boundaries, which restrain the flow. The effects of the boundaries, in the two-dimensional case, are buoyancy, solid blocking, and wake blocking. These effects have been corrected for and the corrections are listed in the computer program (Appendix B).

Since all the integrations over the airfoil were performed using the pressure coefficient data, the corrections to the airfoil characteristics were standard corrections of the tunnel dynamic pressure from Pope (Ref 6:276). The correction factors at the rake were the standard correction factors from Pope and a correction for the effect of the thickness of the rake to the pressure data.

IV. Discussion and Results

Nearly every curve of the airfoil sectional characteristics has a common irregularity, a discontinuity in slope, or re-entrant point at some point on the curve. This re-entrant point was caused by the transition of the boundary layer on the airfoil from laminar to turbulent and was related to the Reynold's Number chosen for the test and the roughness of the airfoil. At some lower Reynold's Number, the boundary layer would have been laminar throughout the range of α and S_F, and at some higher Reynold's Number, the boundary layer would be turbulent over most of the airfoil throughout the range of α and S_F.

At low α's and/or S_F's the boundary layer was laminar, but as α and/or S_F was increased, the local velocity over the airfoil increased, causing the laminar boundary layer to begin to separate. Increasing α and/or S_F then caused the boundary layer to become turbulent and it re-attached, increasing C_L and decreasing C_{D_P}. This argument is supported by the fact that the re-entrant point shifted to lower α's when blowing is applied (Fig. 20). Blowing increased the local velocity, added turbulence, and caused the transition to occur sooner A re-entrant point was obtained by Turner (Ref 8:13) in his smooth-airfoil data curve, while his rough-airfoil data curve was smooth. The rough surface of the airfoil induced turbulent flow at a lower Reynold's Number and the boundary layer was turbulent throughout the range of angle of attacks. The smooth airfoil, however, experienced the transition and the re-entrant point resulted.

The results near stall are questionable, especially at high flap deflections. The model was so large, relative to the tunnel height, that blockage effects exceeded the correction factors at high rotations of the model. Blowing also increased the blockage. Fig. 34 shows that the velocity component of the flow perpendicular to the flap chord at the trailing edge was greatly reduced when blowing was applied. In other words, the free stream was being forced downward by the ejected air, and blocking effects increased. This figure also shows that, near stall, the velocity sharply increased, i.e., the ejected air no longer followed the flap contour and the free-stream air flowed by the trailing edge with nearly the same velocity as the zero blowing case. Therefore, blocking at stall due to blowing nearly ceased to exist.

This decrease in blocking at stall, plus the fact that the ejected air after separation of the boundary layer adds energy to the low-energy wake, caused some peculiar characteristics near stall, especially noticeable in the pressure drag and moment coefficient curves (Figs. 25, 26 and 32).

The profile drag coefficient, determined from rake-pressure data, was calculated to be .0068, and the pressure drag coefficient, determined from airfoil pressure data, was calculated to be .004. The friction or viscous drag coefficient is the difference between the two or .0028. These calculations were performed for the zero blowing, zero flap deflection, and zero angle of attack case. The rake-pressure data proved unreliable for the other cases because of turbulence and shear layers introduced into the flow.

Comparison of Results

The results obtained in this study compared very favorably with the results obtained by other experimentors. The zero blowing data were compared with similar data in Abbott (Ref 1:462) and found to be in close agreement. Also, $C_{\mu crit}$ at a flap deflection of sixty degrees was identical with that in Lachman (Ref 3:468).

Effect of Blowing on the Pressure Distribution

The effects of blowing on the Pressure Distribution were the shifting of the fore and aft stagnation points, the marked decrease in the static pressures over the leading edges of the airfoil and flap, the increase in pressure over the entire bottom surface of the airfoil and flap, and the increase in pressure near the trailing edge of the flap. Blowing, then, caused more of the free-stream air to be deflected over the upper surface of the airfoil and to be discharged from the airfoil more tangentially.

Effect of Blowing on the Sectional Characteristics

The aerodynamic characteristics of the airfoil with the flap deflected 0, 15, 30, 45, and 60 degrees are presented for several values of C_μ in Appendix A. In general, C_L, C_H, and C_{mle} increased with increase in C_μ. The slope of the lift curve was not appreciably effected but C_{D_P} decreased with increase in C_μ. But the induced drag coefficient probably increased because blowing caused an added downwash velocity and the viscous drag coefficient also probably increased because of larger local velocities induced by blowing. Therefore, the change in the total drag coefficient cannot be determined. The angle of stall decreased at lower values of C_μ's, but began to increase in the supercirculation region.

Optimization of C_μ and S_F

For a particular flap deflection the optimum momentum coefficient for the largest increase in C_L per increase in C_μ is $C_{\mu crit}$. (This is important because C_μ is a measure of the power required to blow the flap.) Above $C_{\mu crit}$ the power required to blow the flap to obtain an increase in C_L increases sharply (Fig. 35). The increases in C_L and the percentage increases in C_L (based on zero blowing data) were plotted versus $C_{\mu crit}$ (Fig. 36). From these curves it was determined that a flap deflection of 45 degrees gave the maximum increase in C_L and that flap deflections of 30 and 45 degrees gave the largest percentage increase in C_L.

Therefore, if power is no problem, a flap deflection of 45 degrees is desired for maximum increase in C_L. However, the same percentage increase in C_L is obtained at a flap deflection of 30 degrees at a 25 percent lower C_μ.

V. Conclusions

A wind-tunnel investigation to determine the effect of boundary-layer control by blowing over the trailing edge flap of an NACA 0015 airfoil has indicated the following conclusions:

1. Blowing is an effective method of increasing C_{Lmax} for low-speed operations.
2. The optimum flap deflection for maximum increase in lift per power consumed in blowing is 45 degrees.
3. The optimum flap deflection for maximum percentage increase in lift per power consumed in blowing is 30 degrees.
4. Blowing in the supercirculation region effectively increases the angle of stall and consequently C_{Lmax}.

VI. Recommendations

It is recommended:

1. That more studies be conducted in the negative angle of attack range to determine the angle of zero lift and other characteristics.
2. That studies be conducted at a higher Reynold's Number to determine the effect of blowing on the sectional characteristics.
3. That studies be conducted at higher C_μ's to more fully determine the effects encountered in the supercirculation region.
4. That the surface of the airfoil be roughened to obtain a turbulent boundary layer throughout the range of α and S_F.
5. That a study be made to determine more accurate blockage correction factors for wind-tunnel testing of airfoils with blowing.

Bibliography

1. Abbott, I.H., and A.E. von Doenhoff. Theory of Wing Sections. New York: McGraw-Hill Book Co., Inc., 1949.

2. The American Society of Mechanical Engineers. Flowmeter Computation Handbook. New York: 1961.

3. Attinello, J.S. "Design and Engineering Features of the Flap Blowing Installations," in Boundary Layer and Flow Control, edited by G.V. Lachman. New York: Pergamon Press, 1961, pp. 463-515.

4. Ketter, L.W. Flow Visualization of an NACA 0024 Airfoil With Blowing at the Knee Flap. Unpublished Thesis. Wright-Patterson A.F.B., Ohio: Air Force Institute of Technology, June 1964.

5. Kuethe, A.M., and J.D. Schetzer. Foundations of Aeronautics (Second Edition). New York: John Wiley & Sons, Inc., 1959.

6. Pope, A. Wind-Tunnel Testing (Second Edition). New York: John Wiley & Sons, Inc., 1958.

7. Schlichting, H. Boundary Layer Theory (Fourth Edition). New York: McGraw-Hill Book Co., Inc., 1960.

8. Turner, T.R. Wind Tunnel Investigation of Boundary-Layer Control by Blowing on an NACA 65_5-424 Airfoil to Effect Drag Reduction. NASA Technical Note No. L-3706. Washington: National Aeronautics and Space Administration, May, 1964.

Appendix A

Tabulated Data

TABLE I

LOCATION OF STATIC PRESSURE TAPS ON THE AIRFOIL

($\alpha = 0°$, $S_F = 0°$)

Pressure Tap	$\frac{x}{c}$*	$\frac{y}{c}$**
1	0	0
2,3	.001	± .006947
4,5	.005	± .015266
6,7	.010	± .021296
8,9	.020	± .029498
10,11	.030	± .035502
12,13	.040	± .040346
14,15	.050	± .044418
16,17	.075	± .052499
18,19	.100	± .058535
20,21	.125	± .063193
22,23	.150	± .066815
24,25	.175	± .069610
26,27	.200	± .071720
28,29	.250	± .074266
30,31	.300	± .075022
32,33	.400	± .072538
34,35	.500	± .066175
36,37	.600	± .057042
38,39	.650	± .051656
40,41	.675	± .048785
42,43	.700	± .045799
44,45	.725	± .042705
46	.75	- .039504
47	L.E. of Flap ,	60° from vertical
48	" " " ,	50° " "
49	" " " ,	40° " "
50	" " " ,	30° " "
51	" " " ,	20° " "
52	" " " ,	10° " "
53	.75	+ .039504
54,55	.775	± .036198
56,57	.800	± .032789
58,59	.825	± .029276
60,61	.850	± .025658
62,63	.900	± .018097
64,65	.950	± .010082
66	1.000	0

* Horizontal distance from L.E. of airfoil.

** Vertical distance from chord line positive up.

TABLE II

VARIATION OF EFFECTIVE SLOT WIDTH

WITH FLAP DEFLECTION

Flap Deflection (Degrees)	0	15	30	45	60
Effective Slot Width (inches)	.034	.0137	.01	.0078	.0081

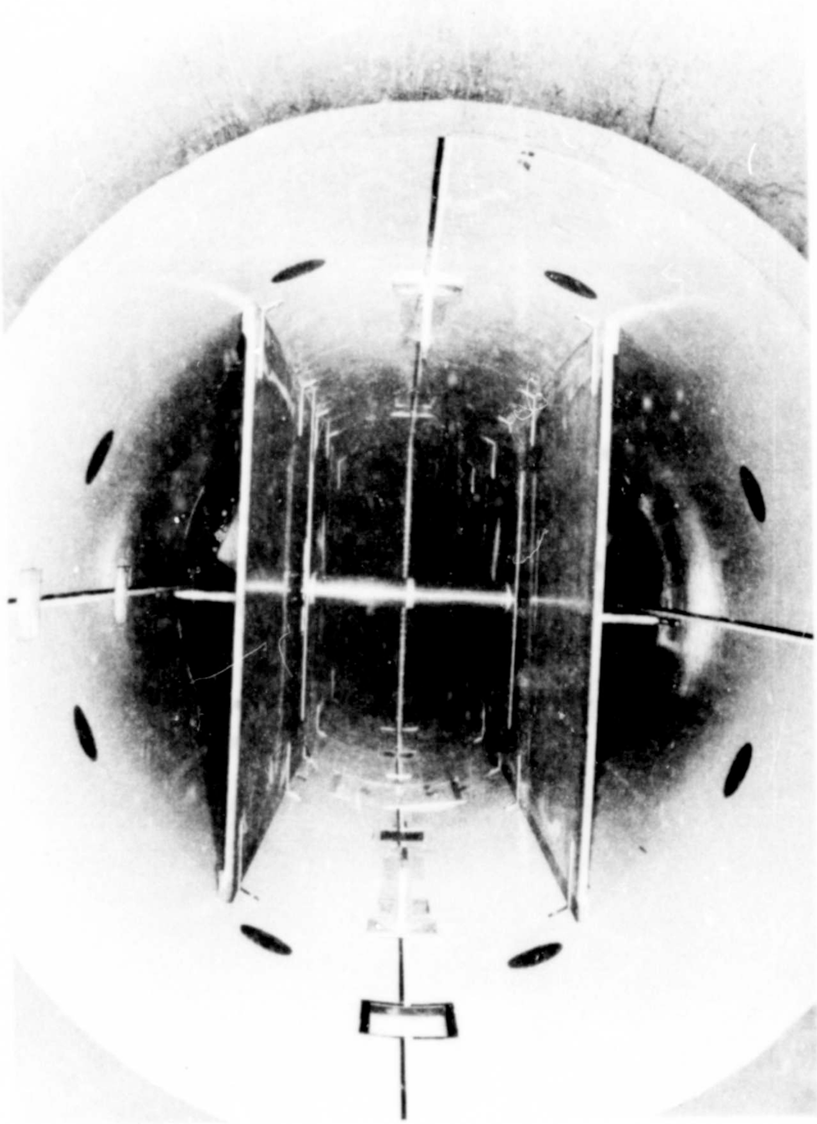

Fig. 1 Front View of Test Section

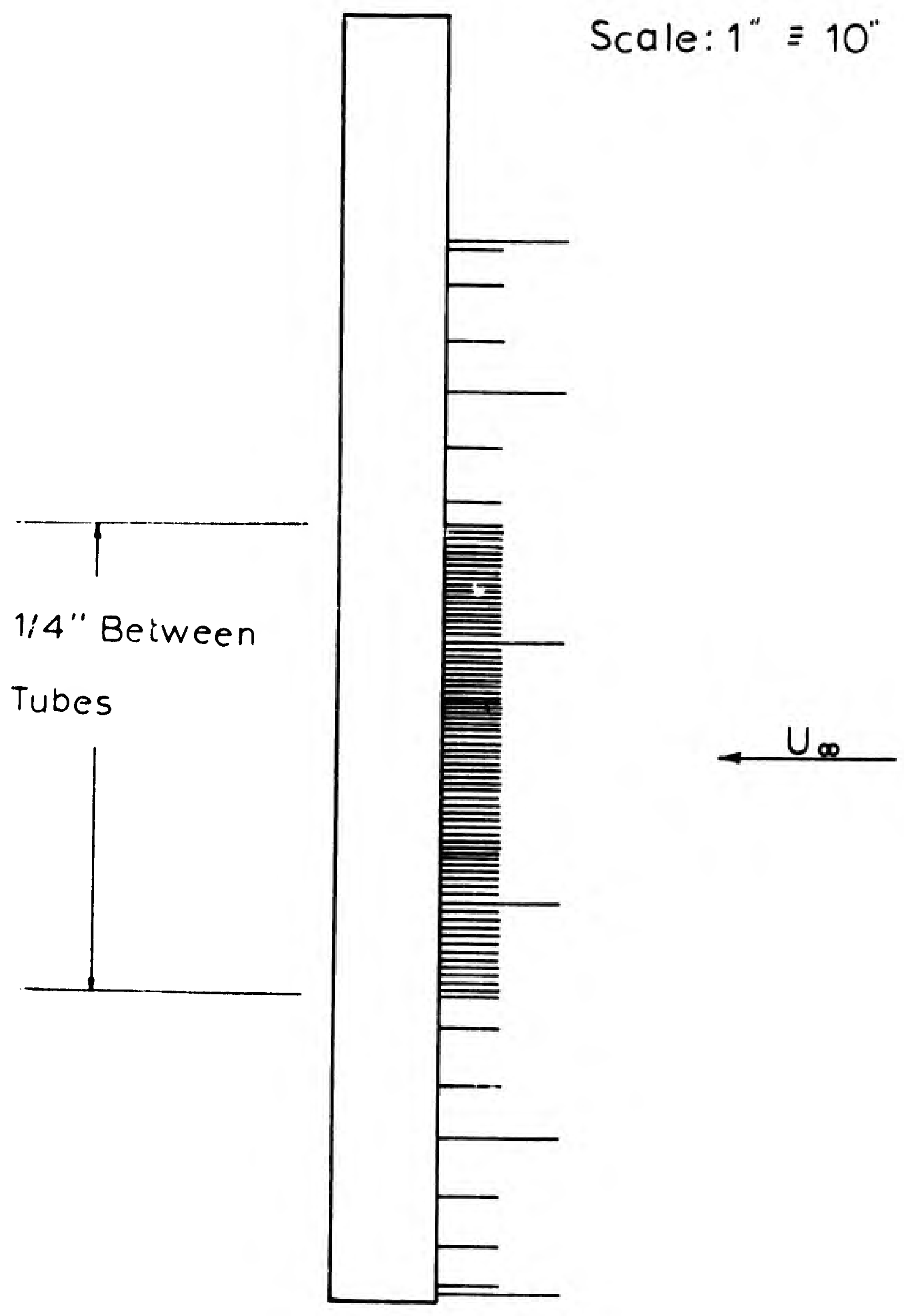

Fig. 2 Survey Rake

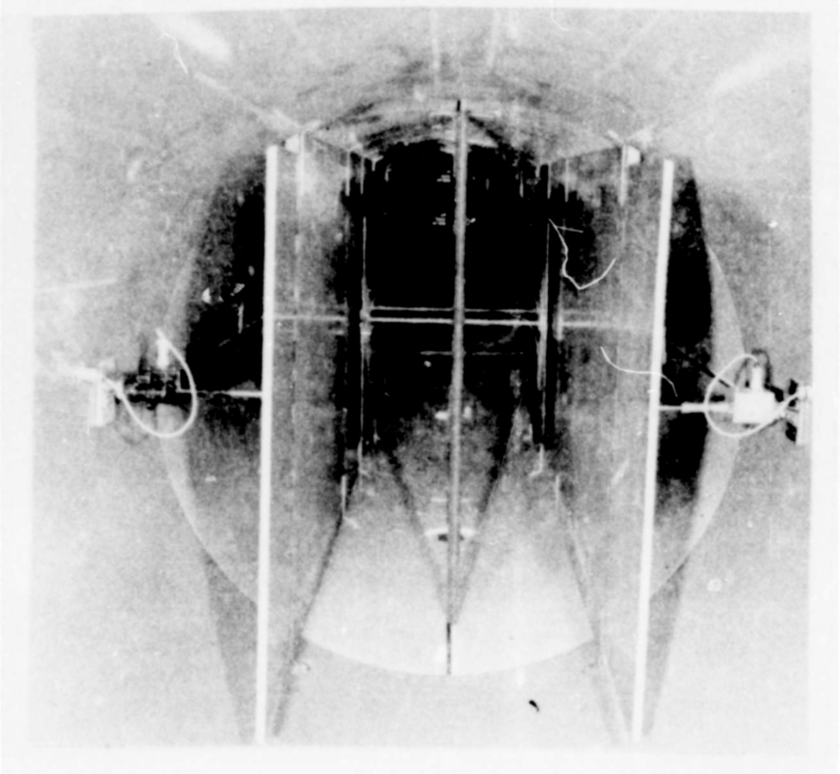

Fig. 3 Rear View of Test Section

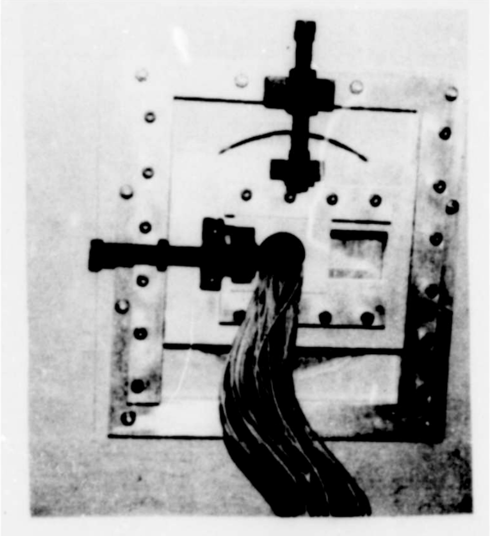

Fig. 4 Traversing Mechanism (Rt.)

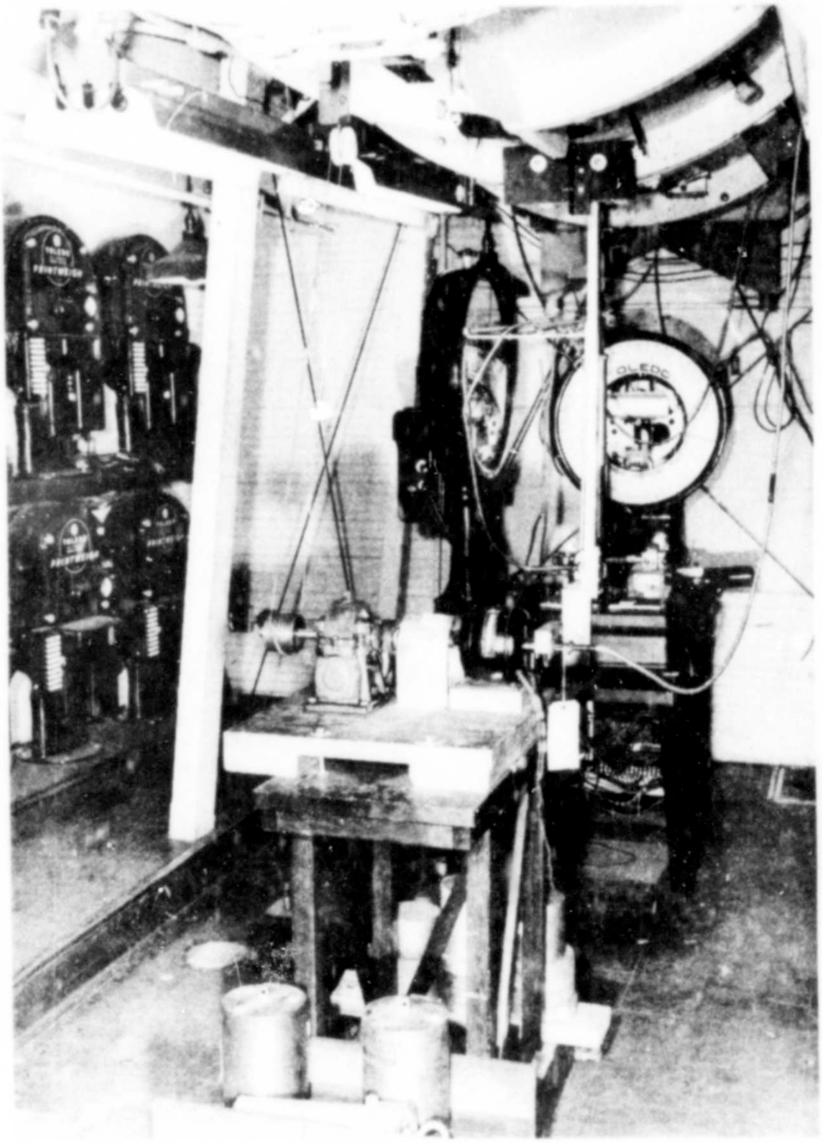

Fig. 5 Angle of Attack Drive Mechanism

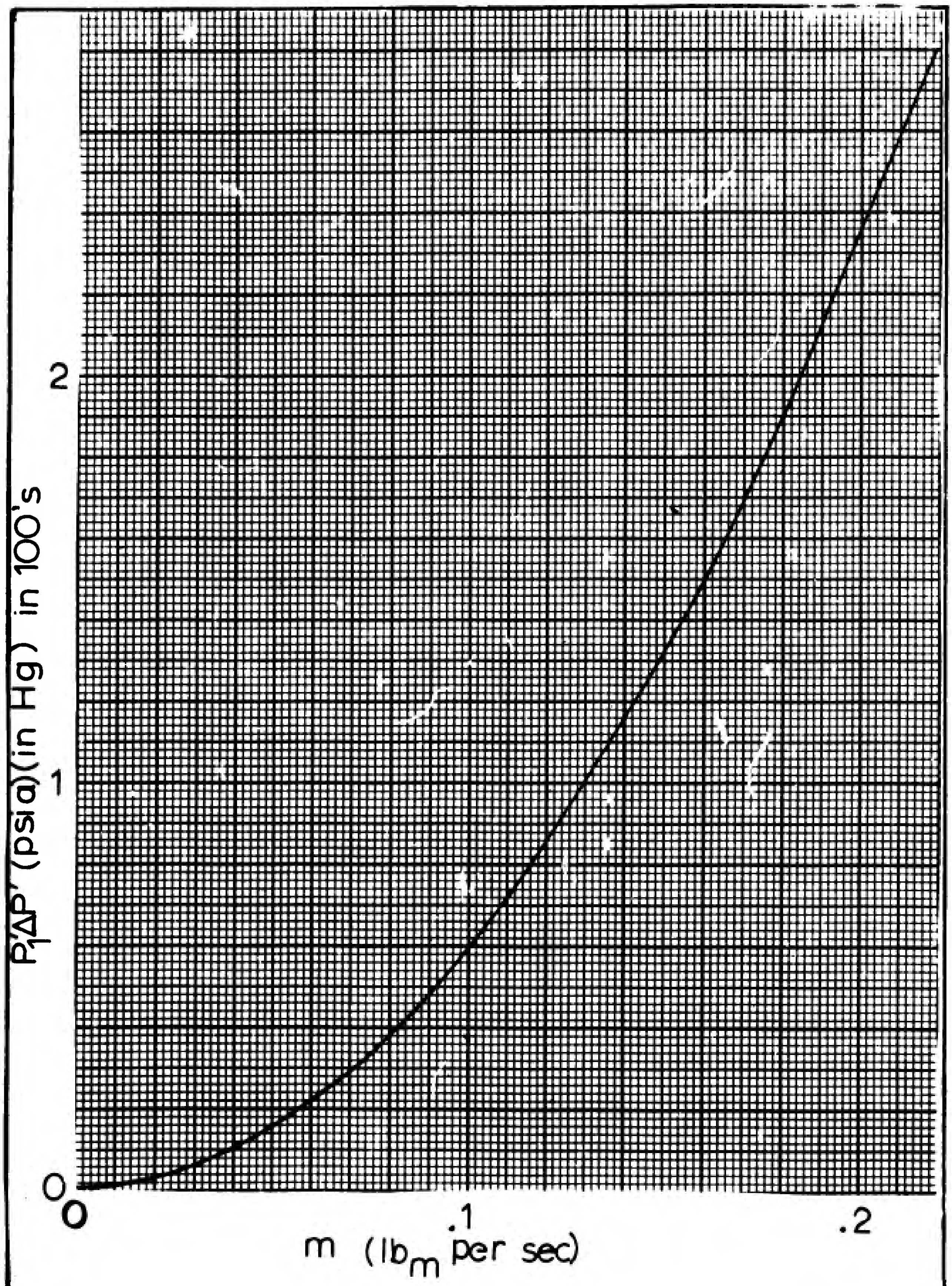

Fig.6 Calibration of 1" D. Flowmeter

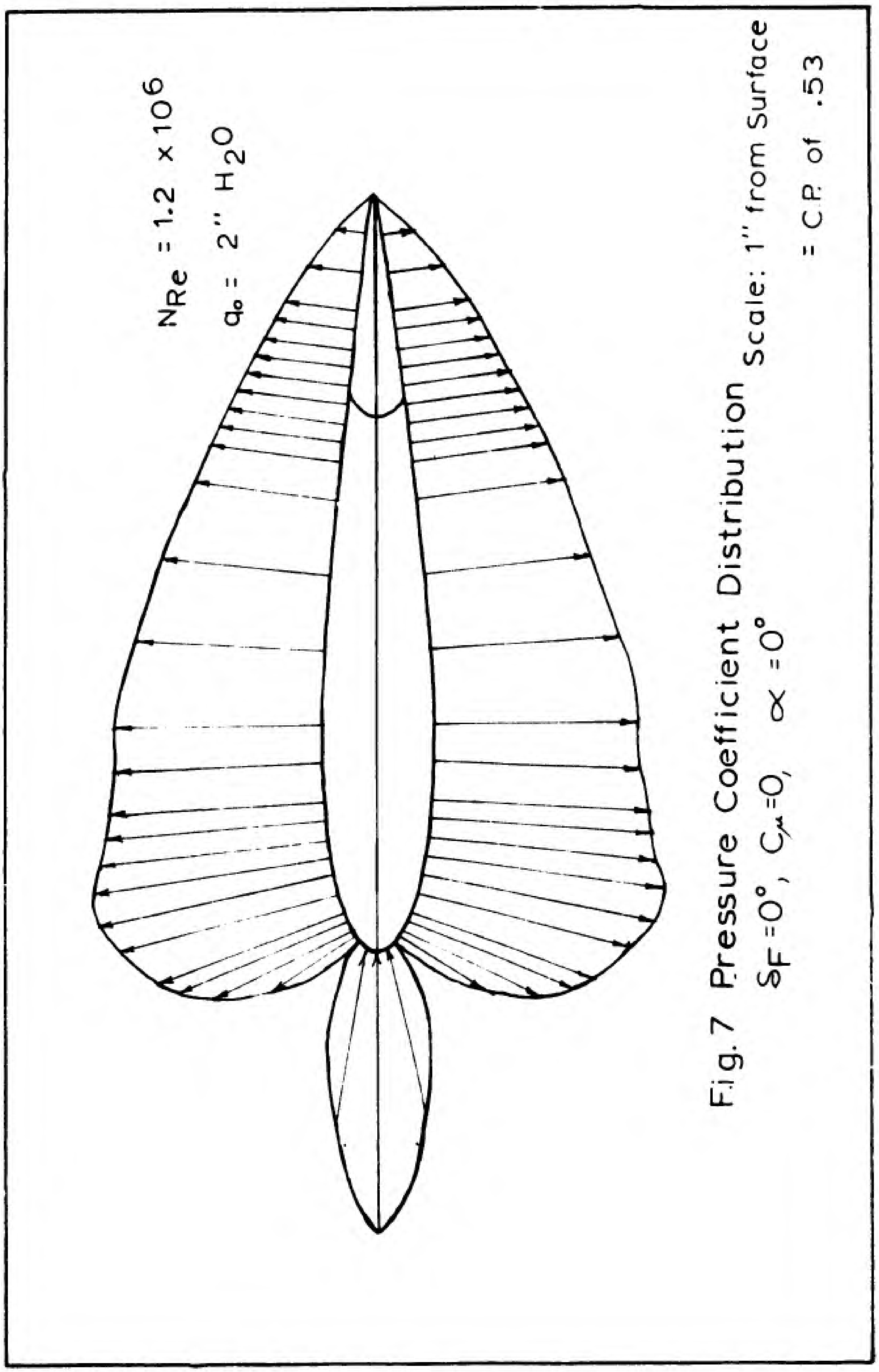

Fig. 7 Pressure Coefficient Distribution
$\delta_F = 0°$, $C_\mu = 0$, $\alpha = 0°$

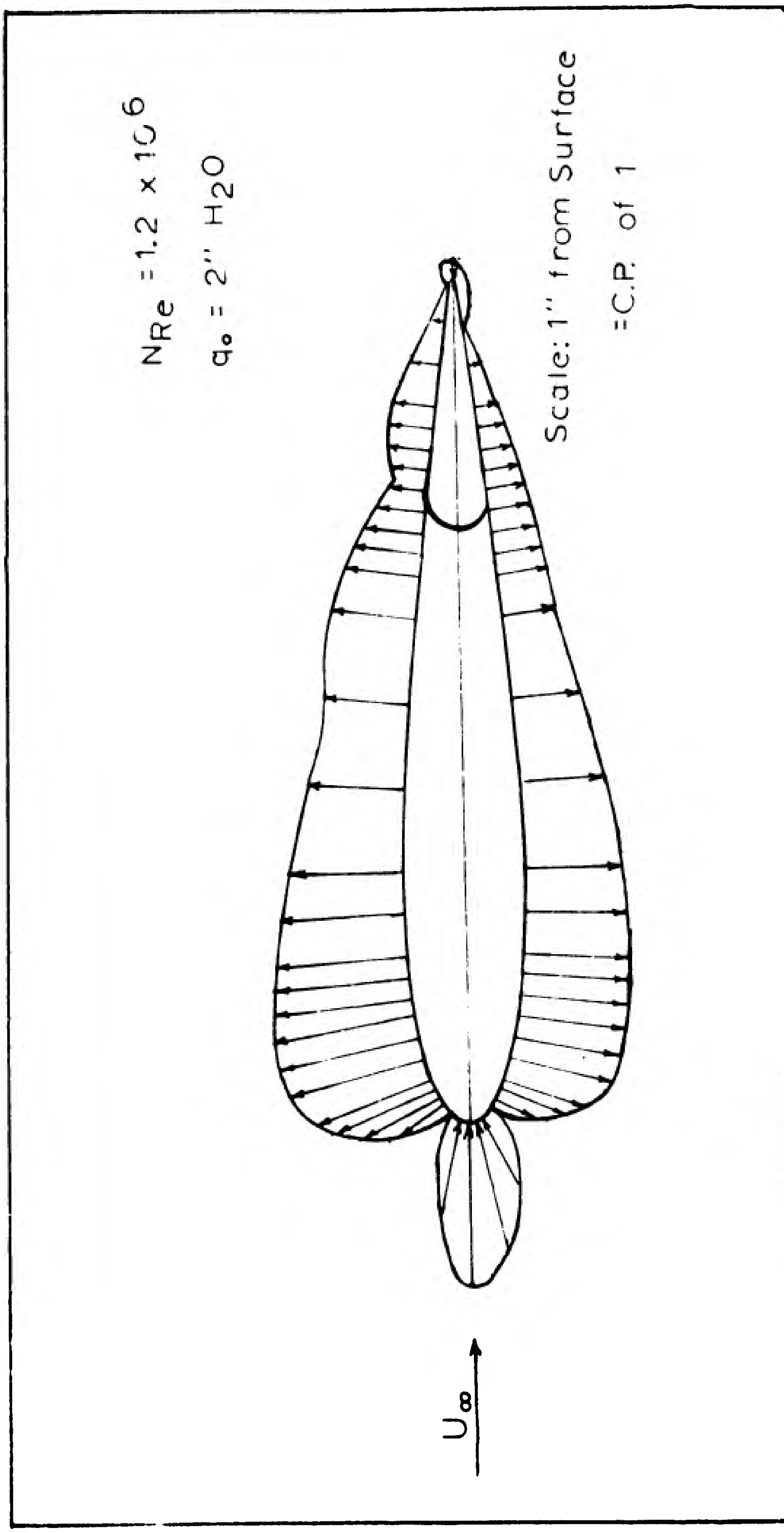

Fig. 8 Pressure Coefficient Distribution
$\delta_F = 0°$, $C_\mu = .033$, $\alpha = 0°$

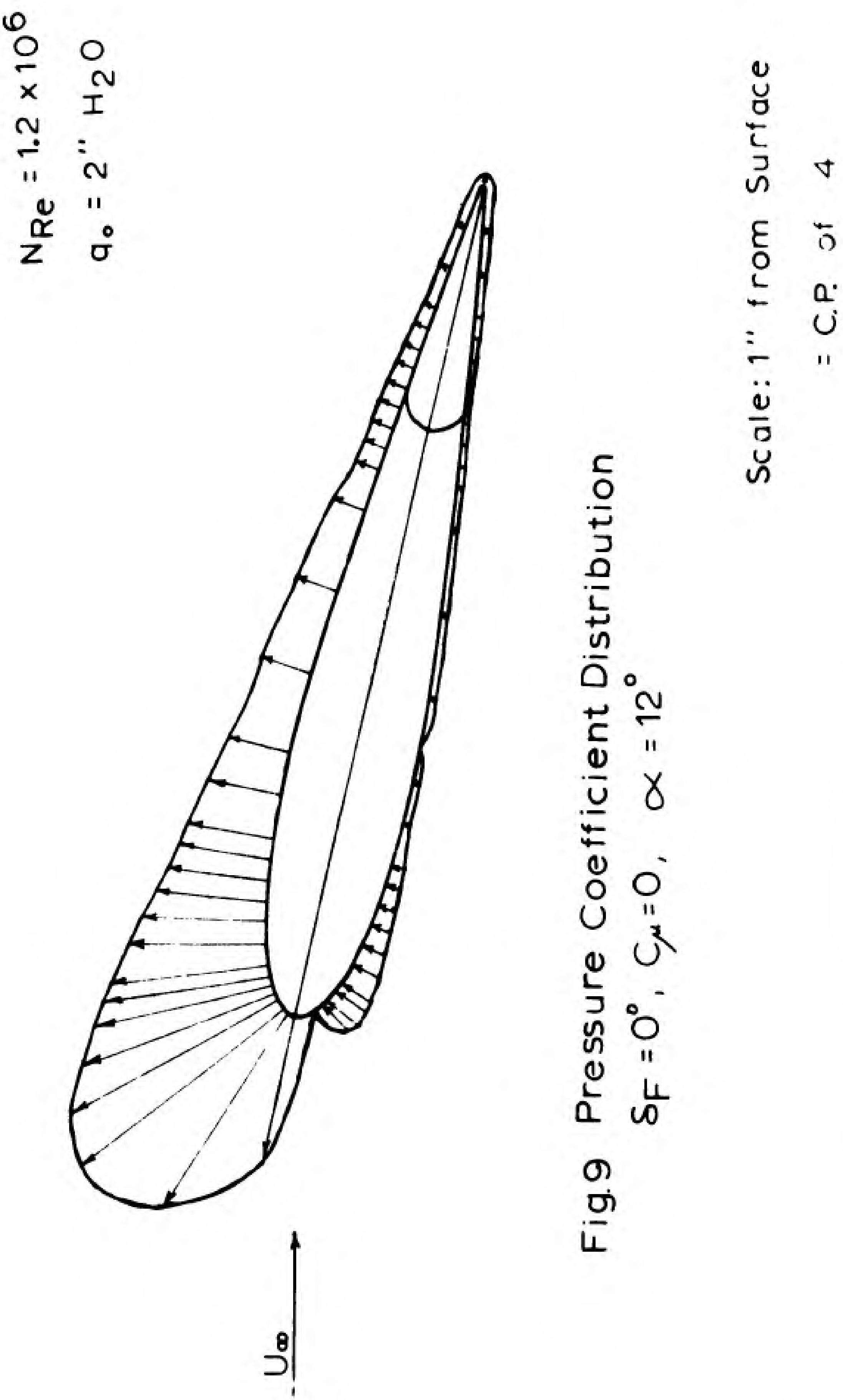

Fig. 9 Pressure Coefficient Distribution
$\delta_F = 0°$, $C_\mu = 0$, $\alpha = 12°$

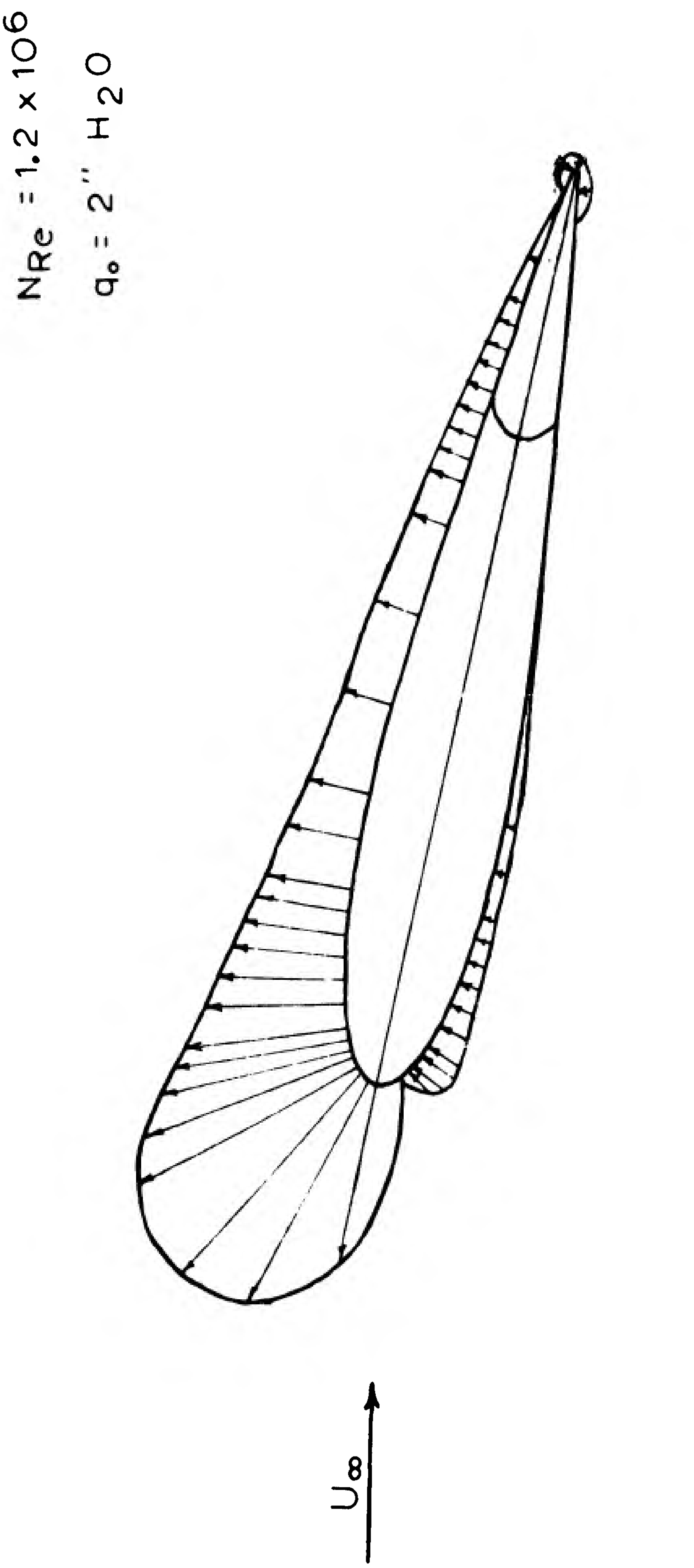

Fig.10 Pressure Coefficient Distribution
$\delta_F = 0°$, $C_\mu = .033$, $\alpha = 12°$ Scale: 1" from Surface = C.P. of 4.8

$N_{Re} = 1.2 \times 10^6$

$q_o = 2''\ H_2O$

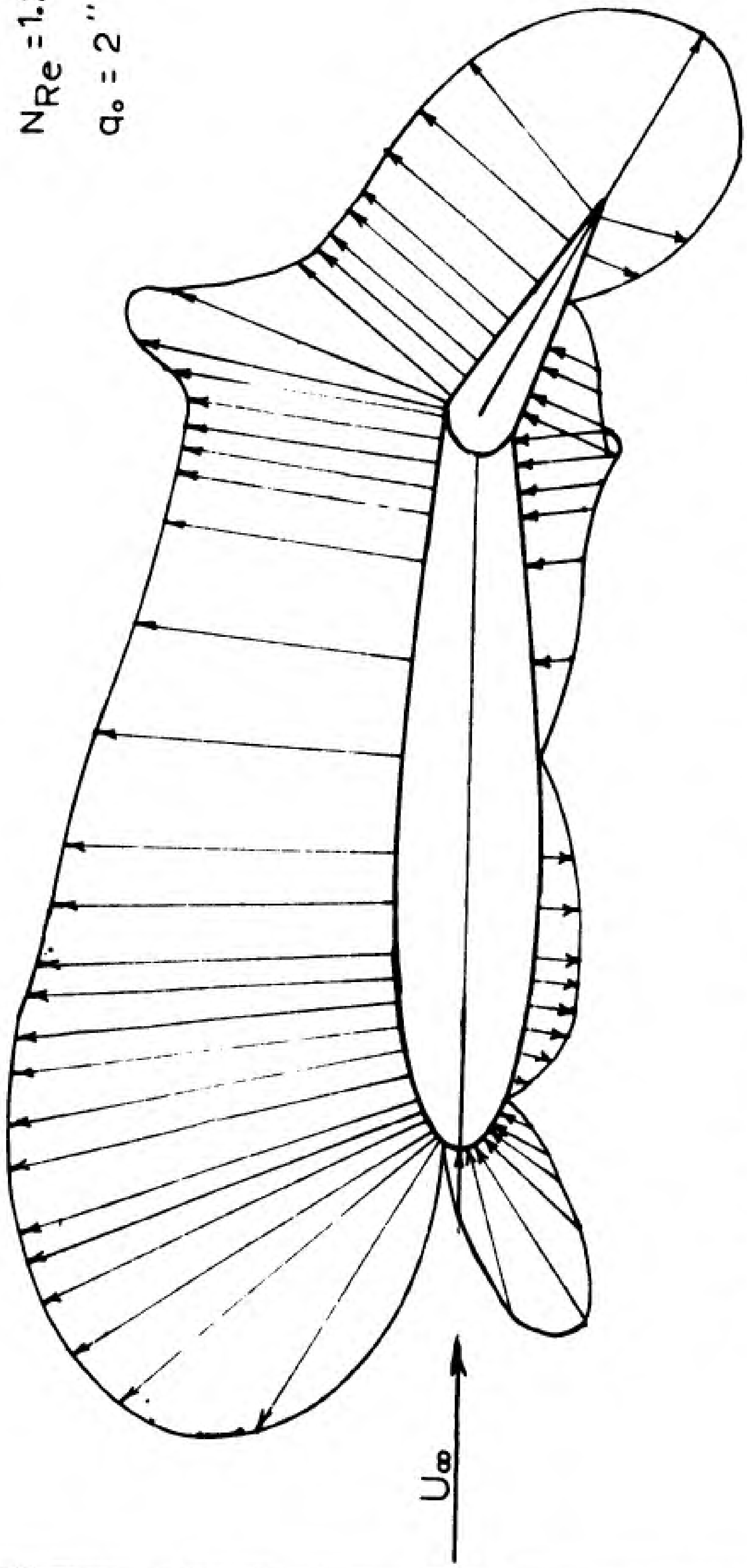

Fig.11 Pressure Coefficient Distribution
$\delta_F = 30°,\ C_\mu = 0,\ \alpha = 0°$

Scale: 1'' from Surface
= C.P. of 1.4

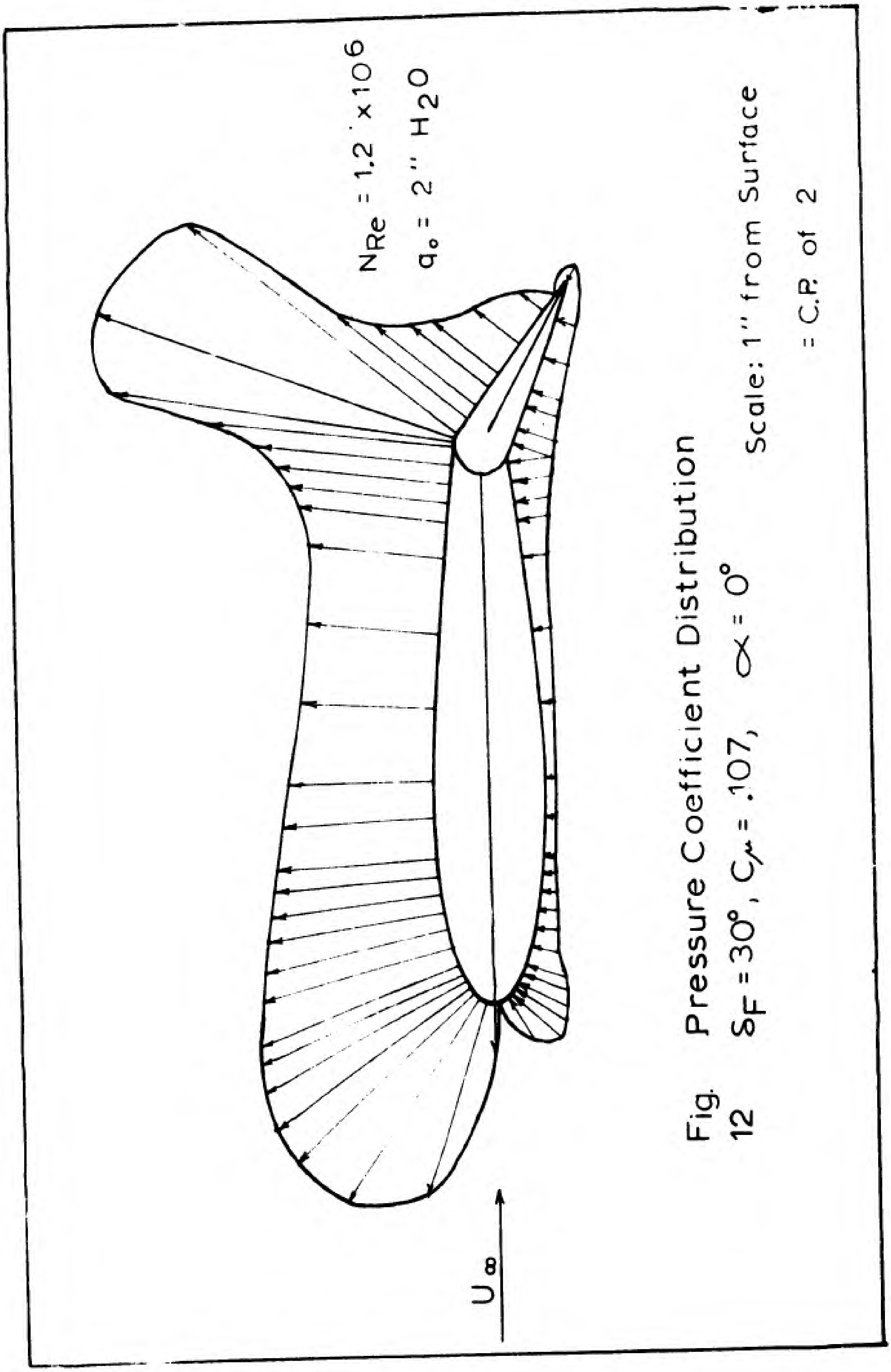

Fig. 12 Pressure Coefficient Distribution
$\delta_F = 30°$, $C_\mu = .107$, $\alpha = 0°$

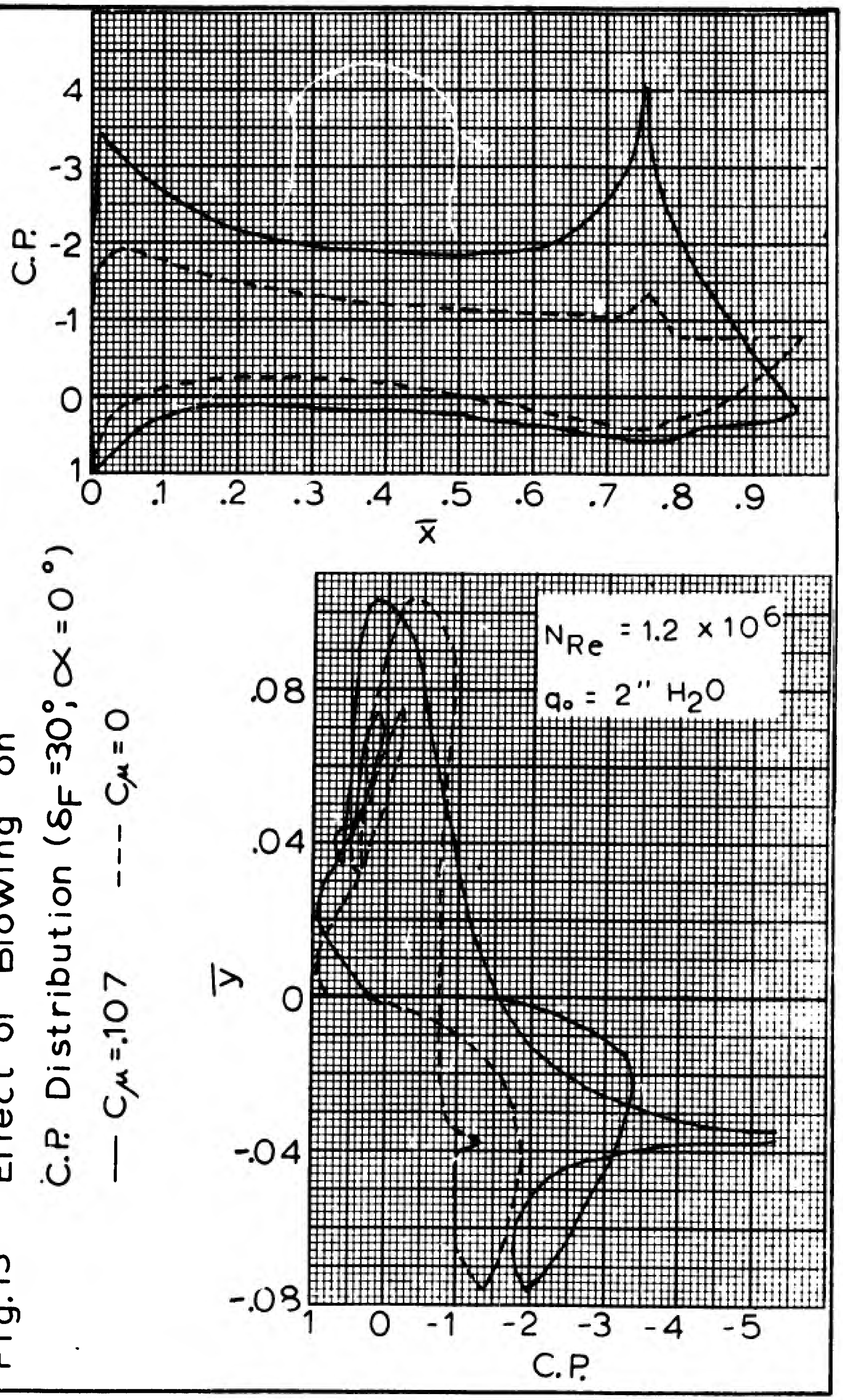

Fig.13 Effect of Blowing on C.P. Distribution (δ_F = 30°, α = 0°)

— C_μ = .107 --- C_μ = 0

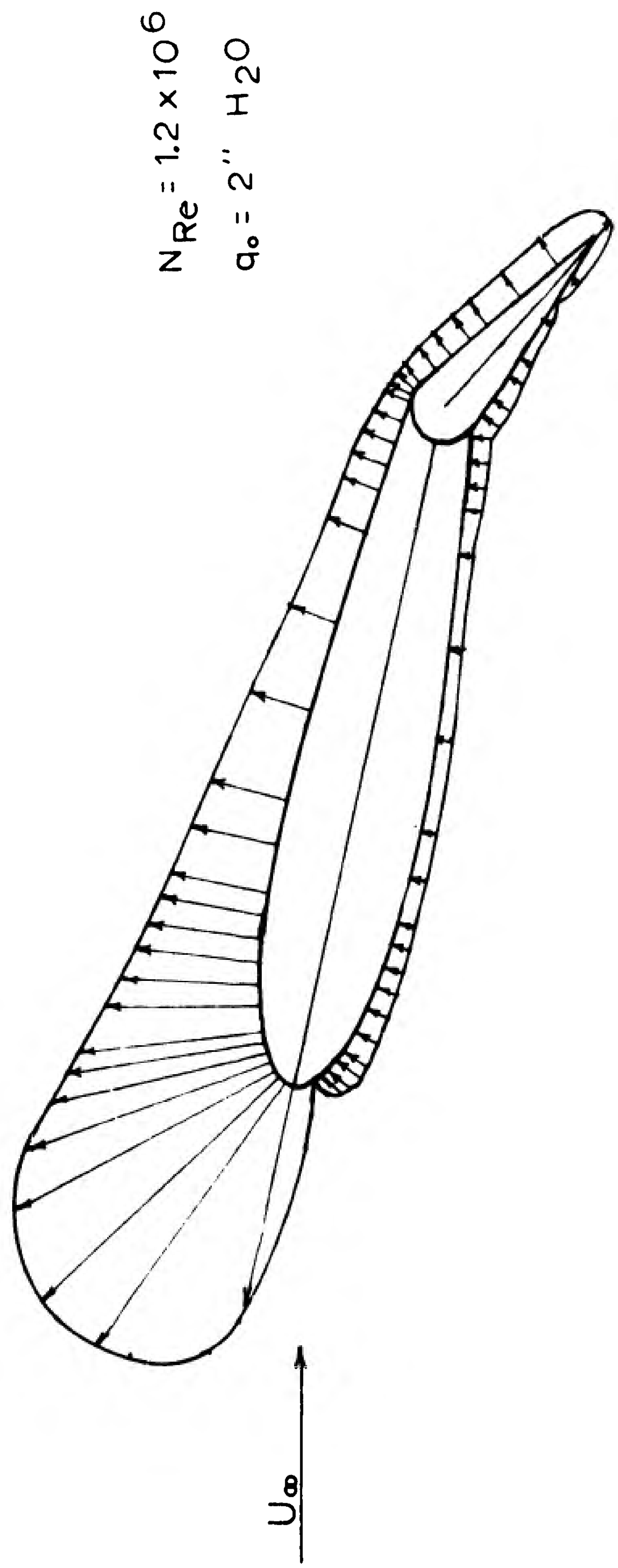

Fig 14 Pressure Coefficient Distribution

$\delta_F = 30°$, $C_\mu = 0$, $\alpha = 12°$

Scale: 1'' from Surface = C.P. of 5.6

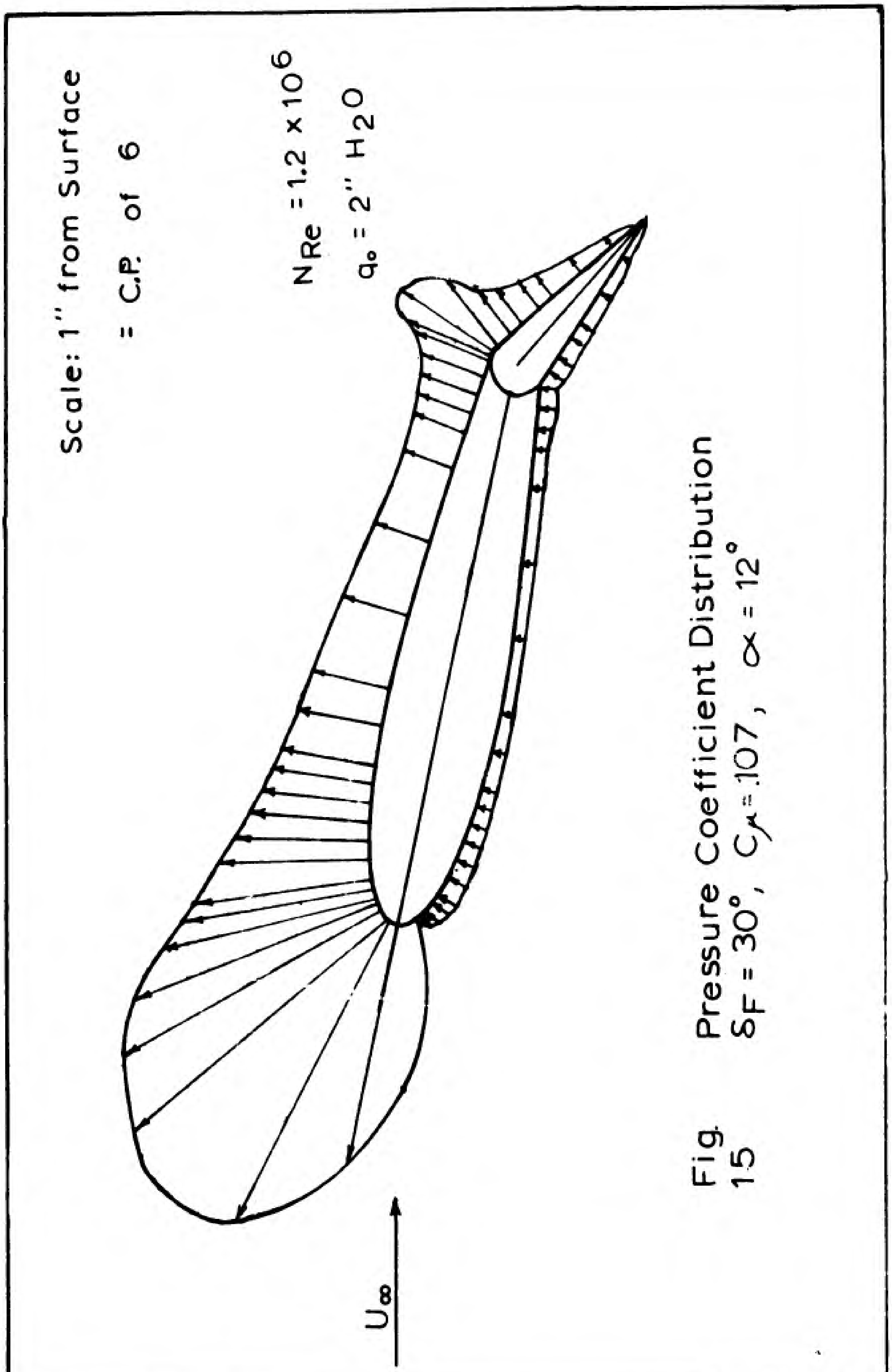

Fig. 15 Pressure Coefficient Distribution
$\delta_F = 30^\circ$, $C_\mu = .107$, $\alpha = 12^\circ$

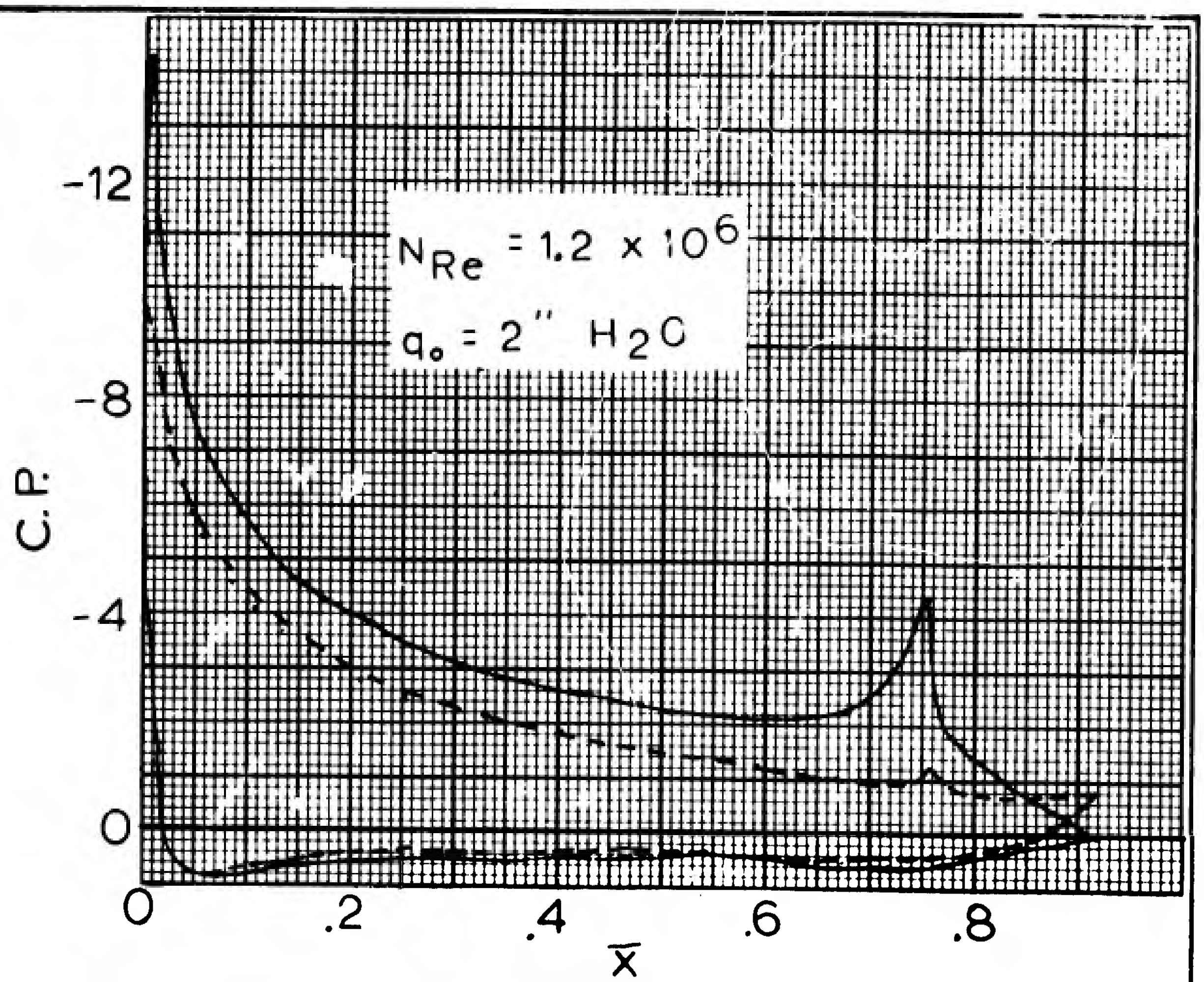

Fig. 16 Effect of Blowing on C.P. Distribution ($\delta_F = 30°$, $\alpha = 12°$)

---- $C_\mu = 0$ ——— $C_\mu = .107$

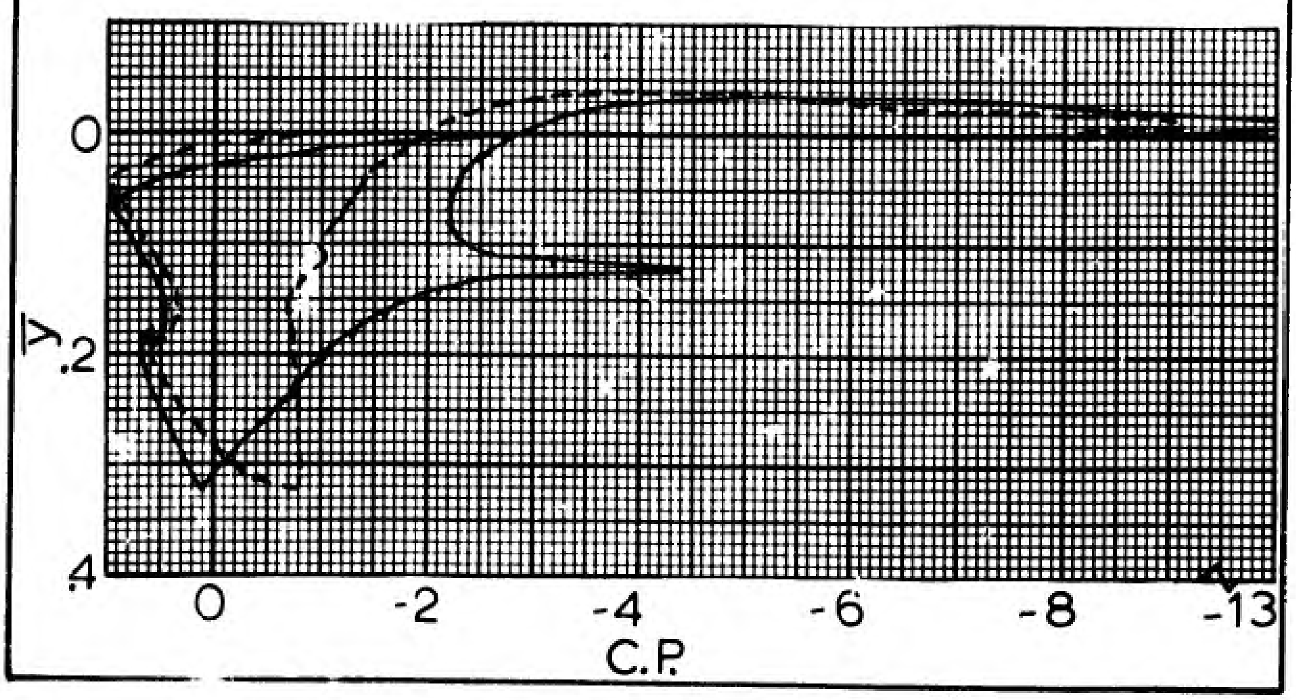

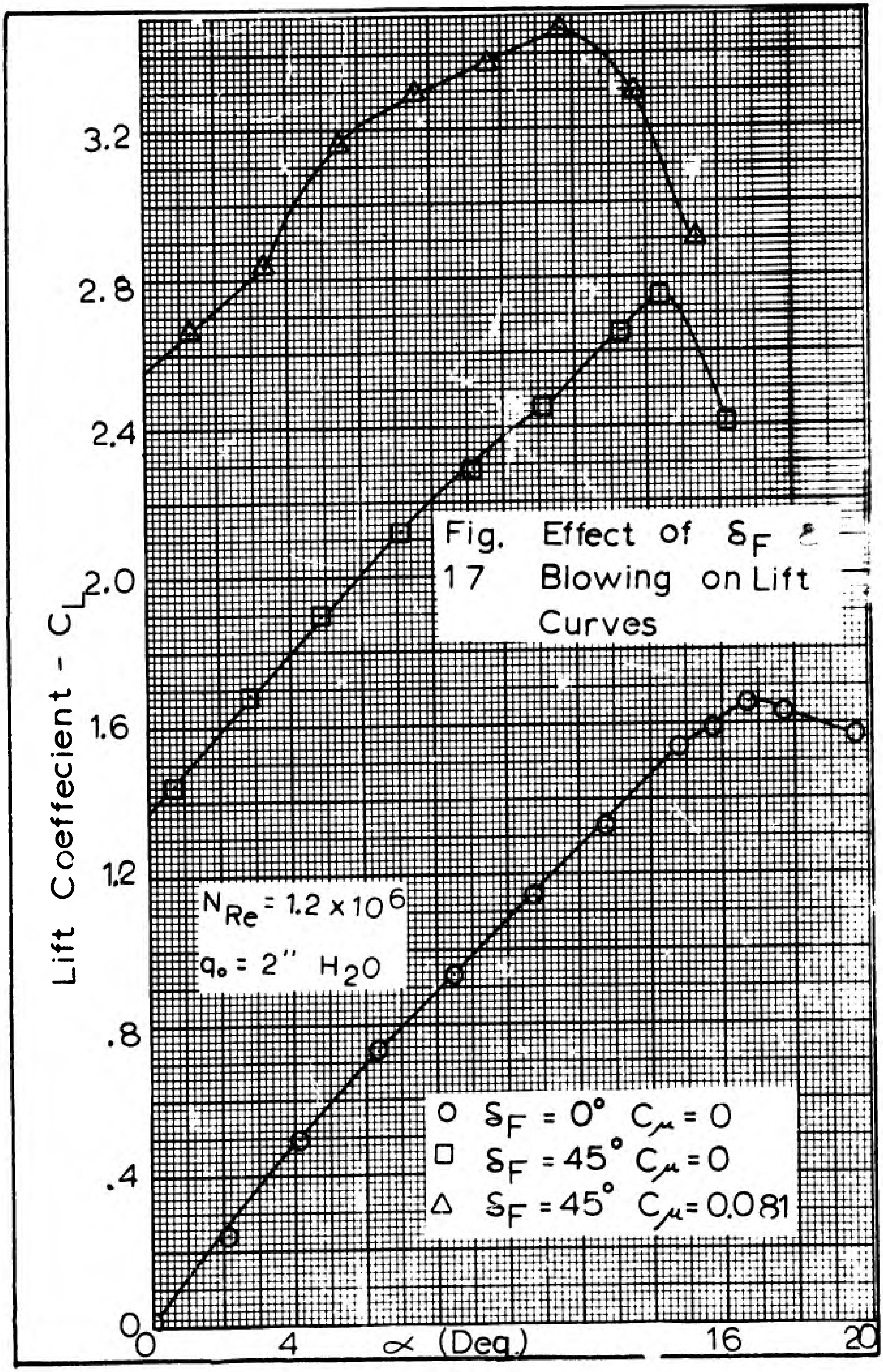
3.2
2.8
2.4
2.0
1.6
1.2
.8
.4
0
Lift Coeffecient - C_L
0
4
16
20
α (Deg.)
Fig. 17 Effect of δ_F & Blowing on Lift Curves
$N_{Re} = 1.2 \times 10^6$
$q_o = 2''$ H_2O
○ $\delta_F = 0°$ $C_\mu = 0$
□ $\delta_F = 45°$ $C_\mu = 0$
△ $\delta_F = 45°$ $C_\mu = 0.081$

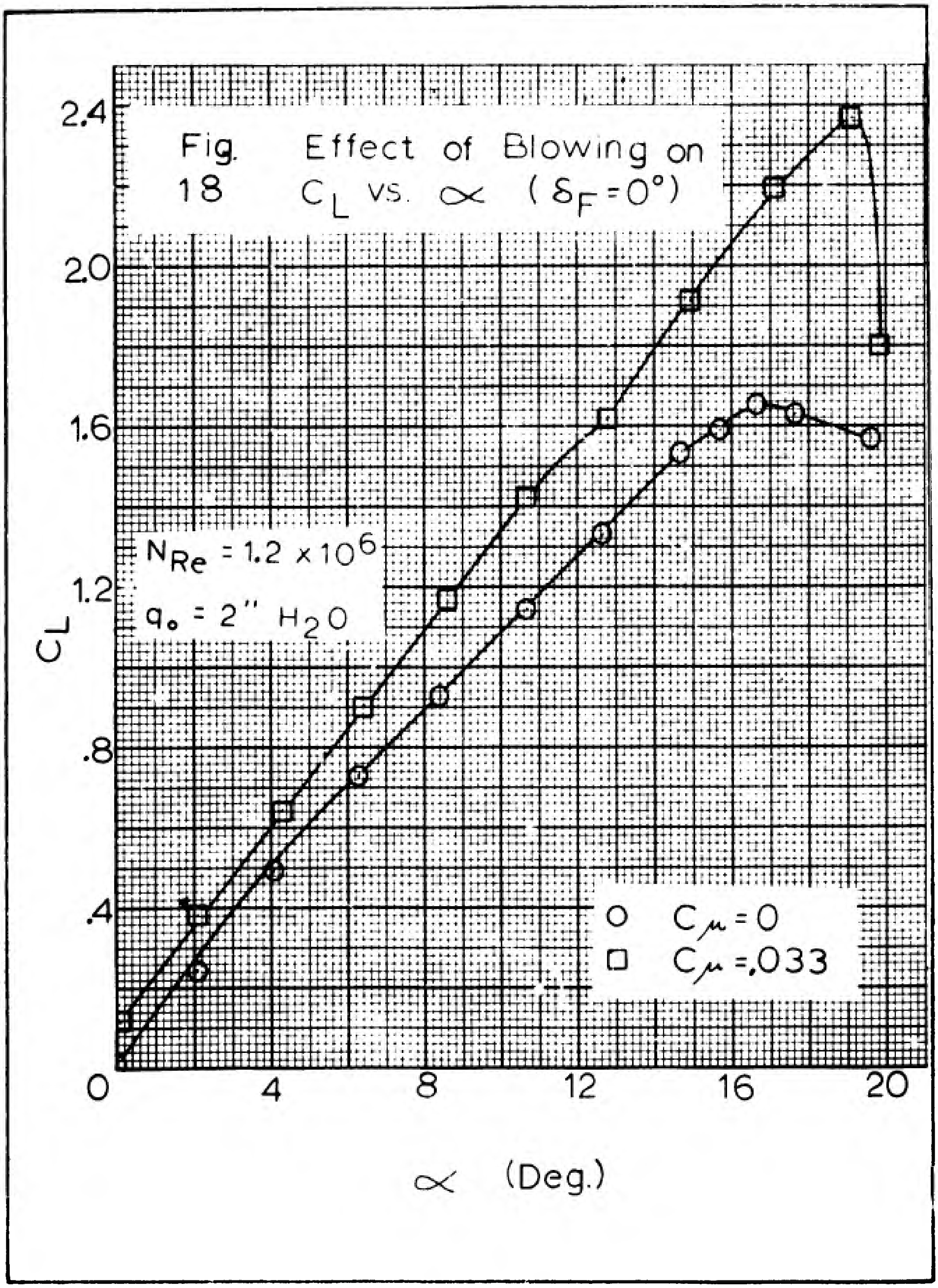
Fig. 18 Effect of Blowing on C_L vs. α ($\delta_F = 0°$)
$N_{Re} = 1.2 \times 10^6$
$q_o = 2''$ H_2O
○ $C_\mu = 0$
□ $C_\mu = .033$
2.4
2.0
1.6
1.2
.8
.4
0
4
8
12
16
20
C_L
α (Deg.)

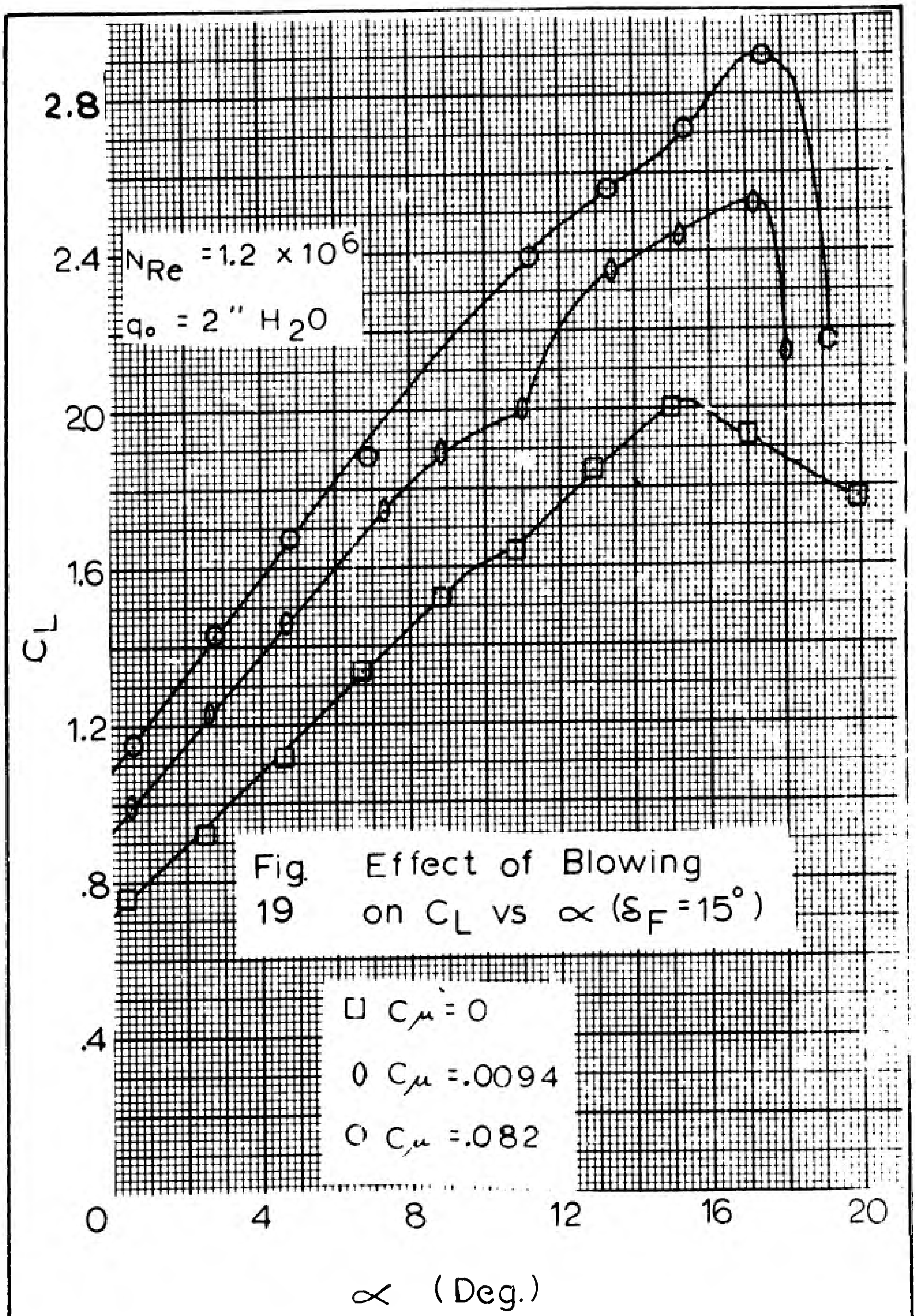

Fig. 19 Effect of Blowing on C_L vs α ($\delta_F = 15°$)

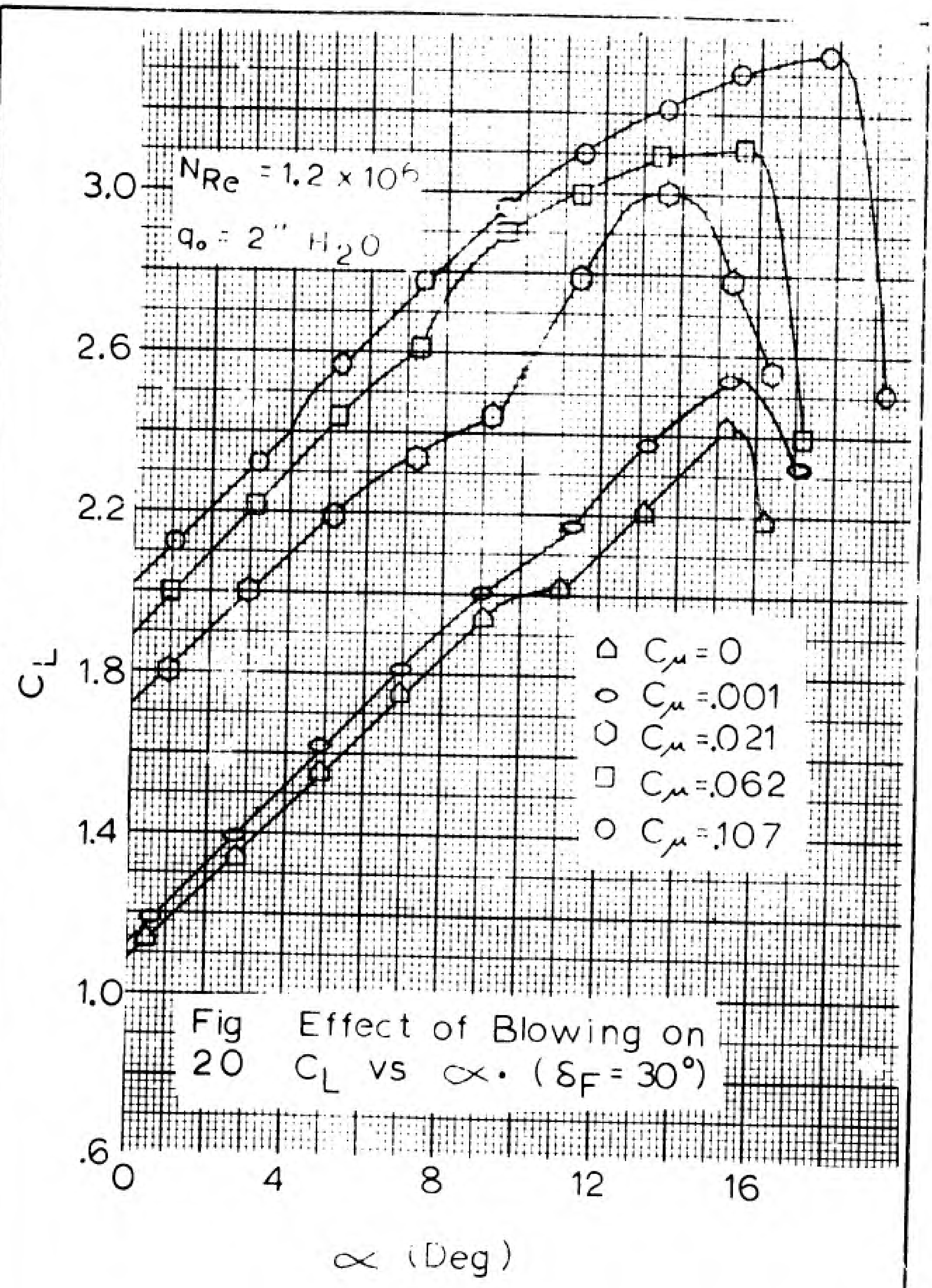

Fig 20 Effect of Blowing on C_L vs α. ($\delta_F = 30°$)

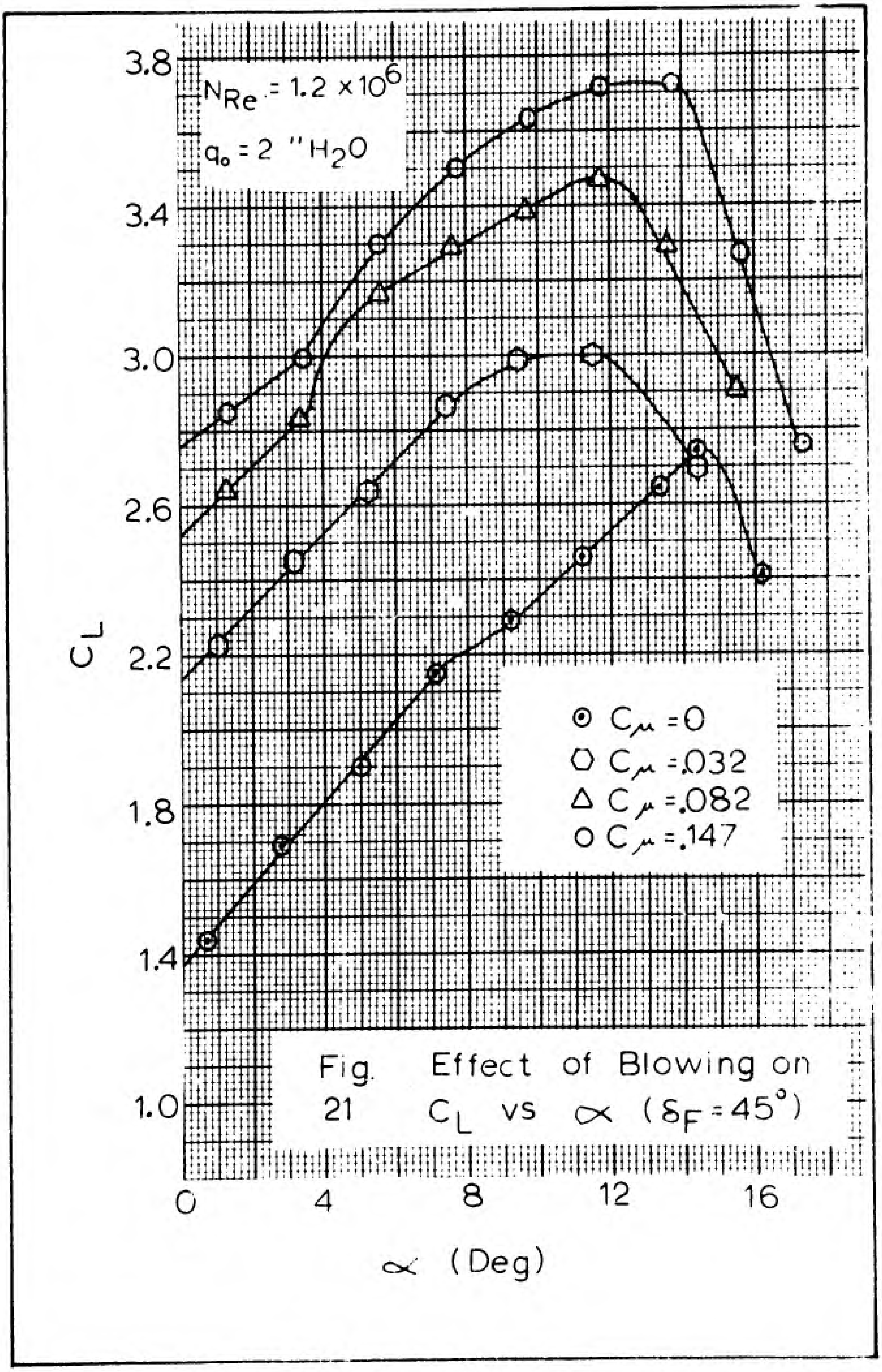

Fig. 21 Effect of Blowing on C_L vs α ($\delta_F = 45°$)

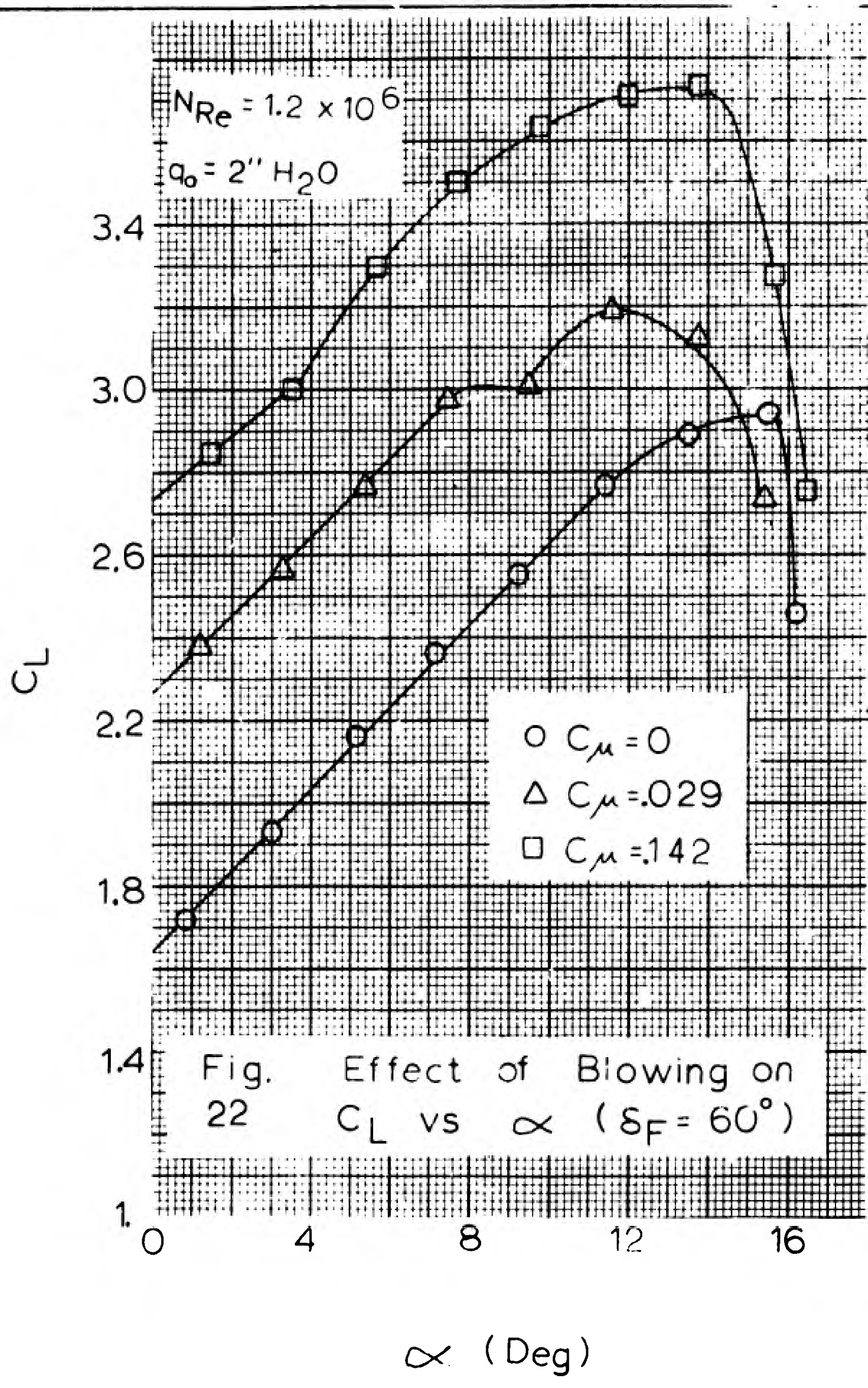

Fig. 22 Effect of Blowing on C_L vs α ($\delta_F = 60°$)

Fig. 23 Effect of Blowing on C_{Dp} at $\delta_F = 0°$ & $15°$

$N_{Re} = 1.2 \times 10^6$

$q_o = 2''\ H_2O$

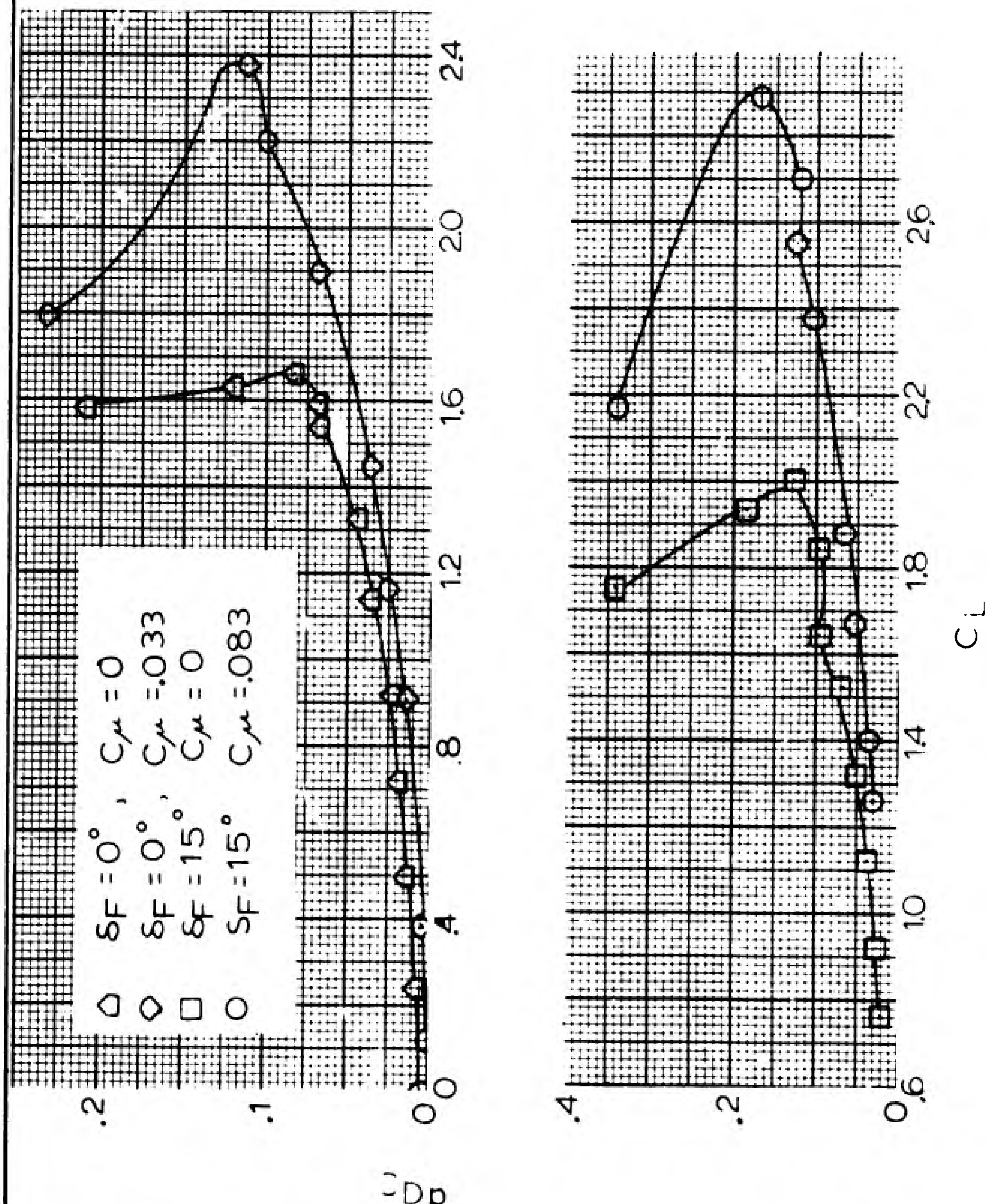

Fig. 24 Effect of Blowing on C_{Dp} ($\delta_F = 30°$ & $45°$)

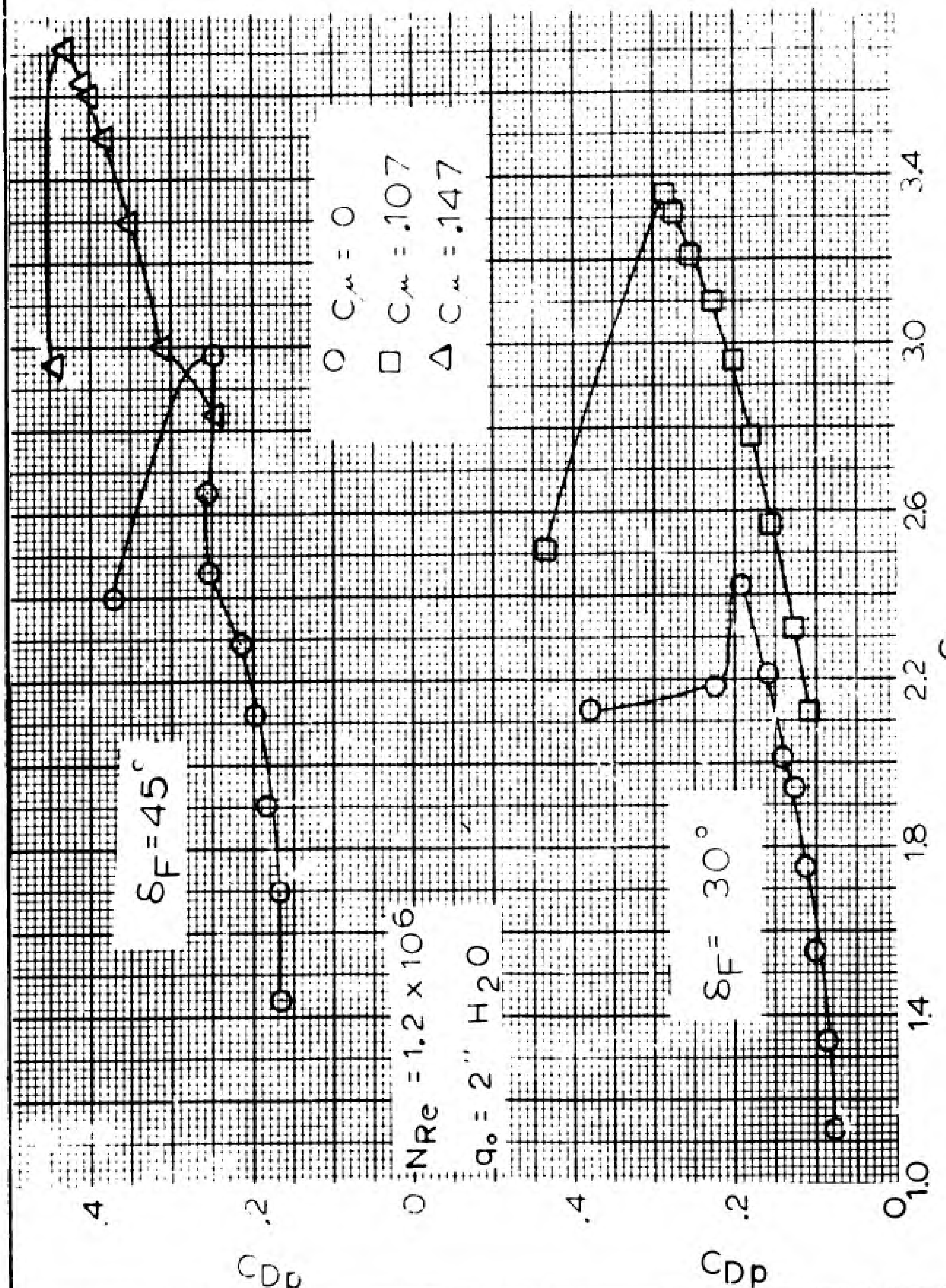

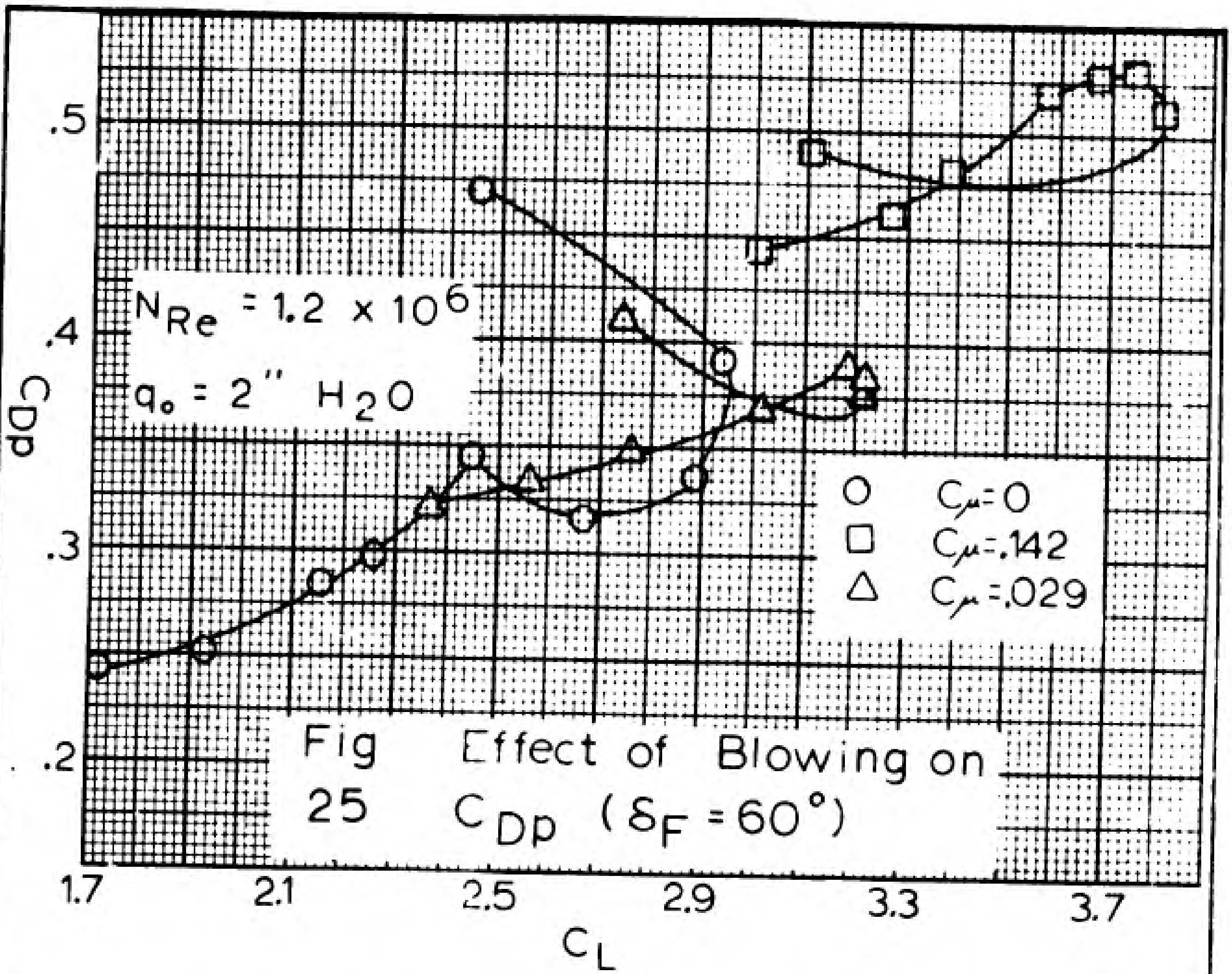

Fig 25 Effect of Blowing on C_{Dp} (δ_F = 60°)

Fig.26 Effect of Blowing on C_H (δ_F = 60°)

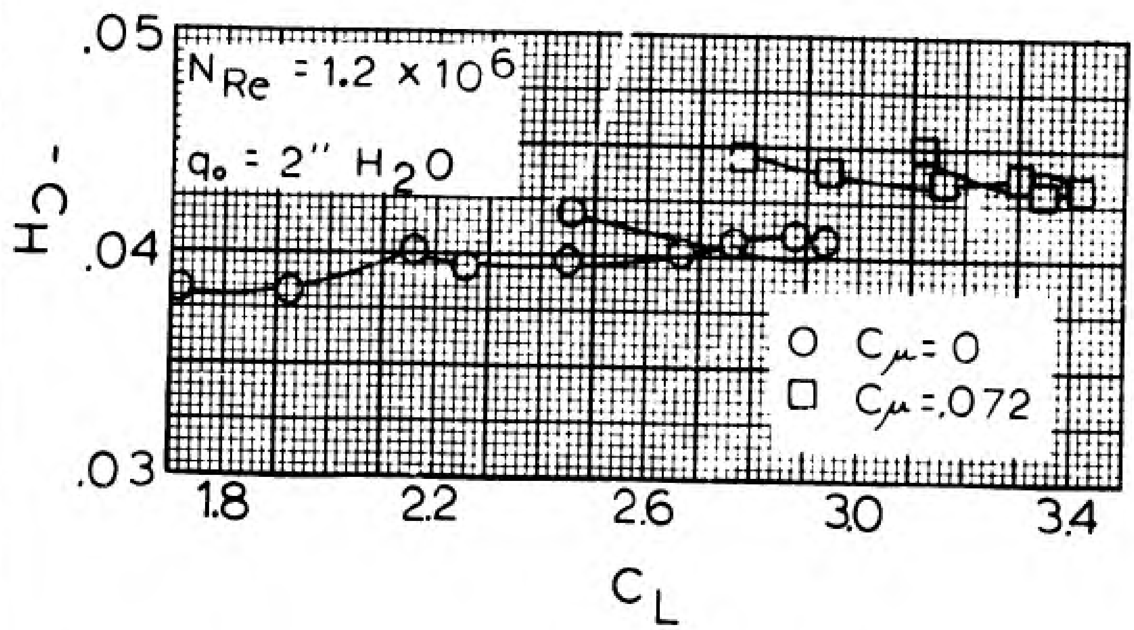

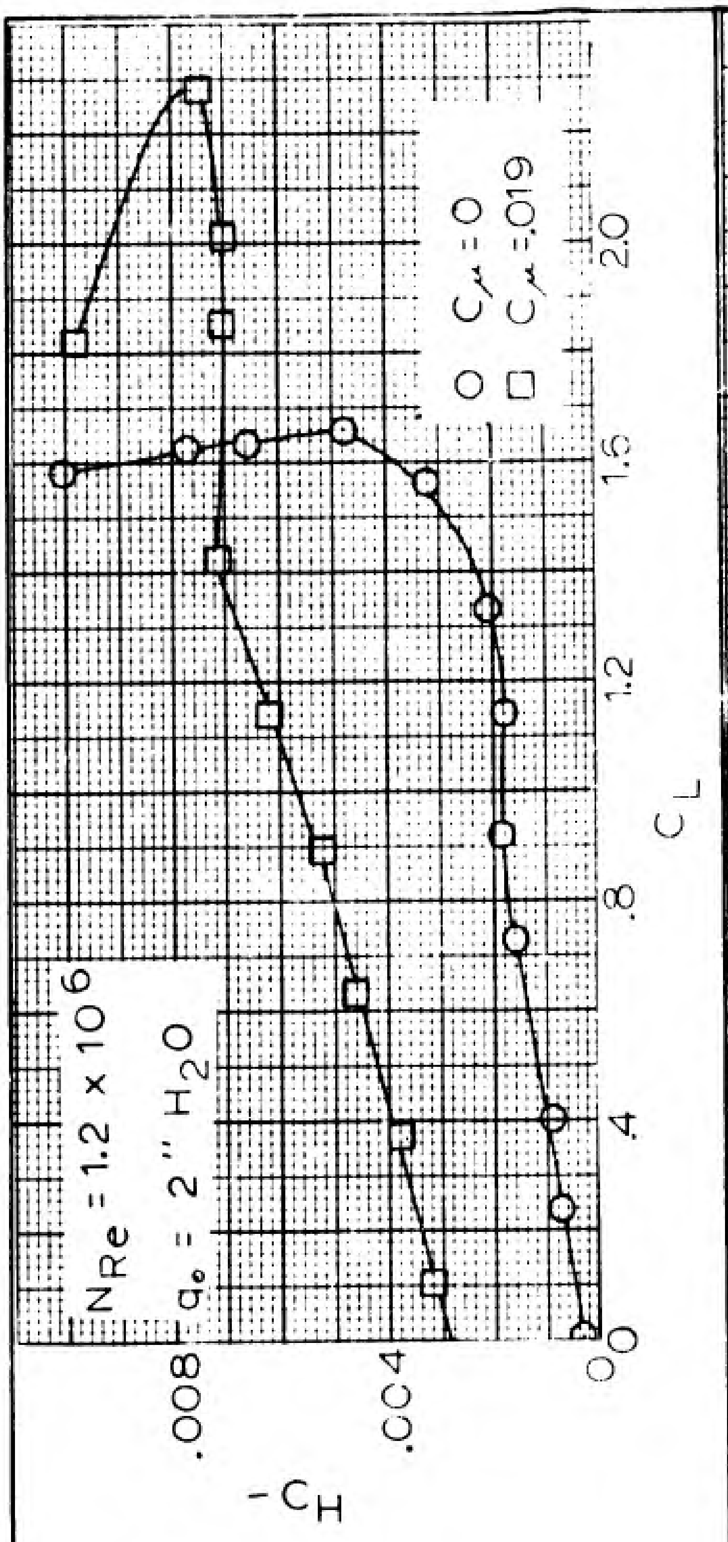

Fig. 27 Effect of Blowing on C_H ($\delta_F = 0°$)

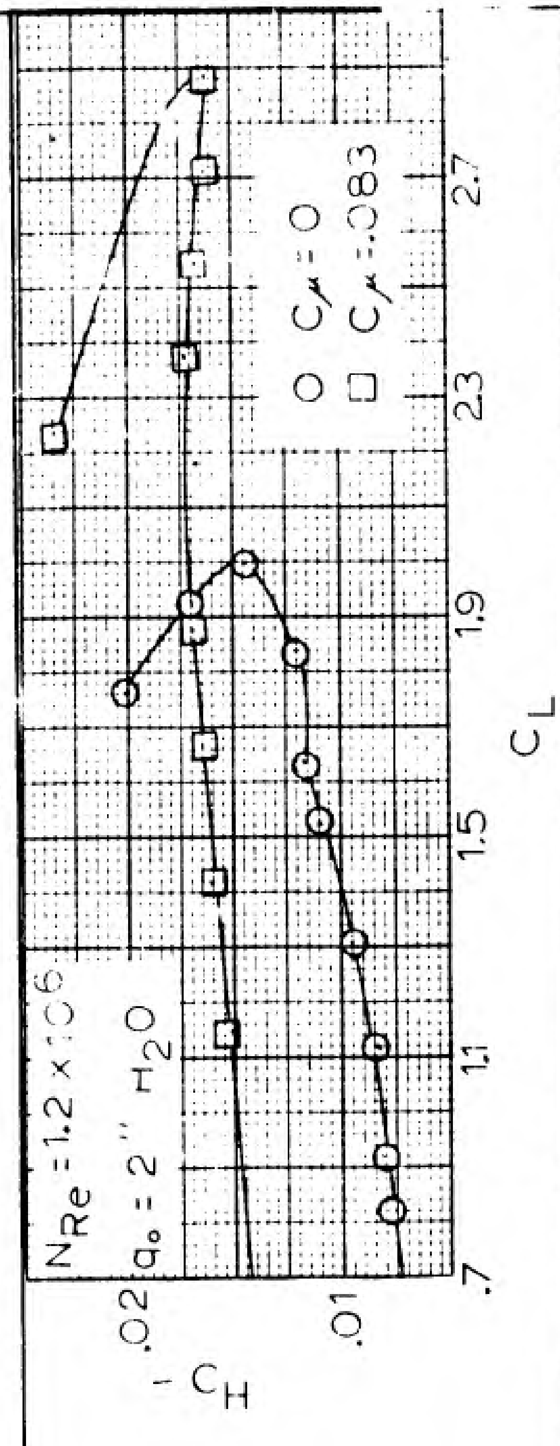

Fig. 28 Effect of Blowing on C_H ($\delta_F = 15°$)

Fig. 29 Effect of Blowing on C_H ($\delta_F = 30°$ & $45°$)

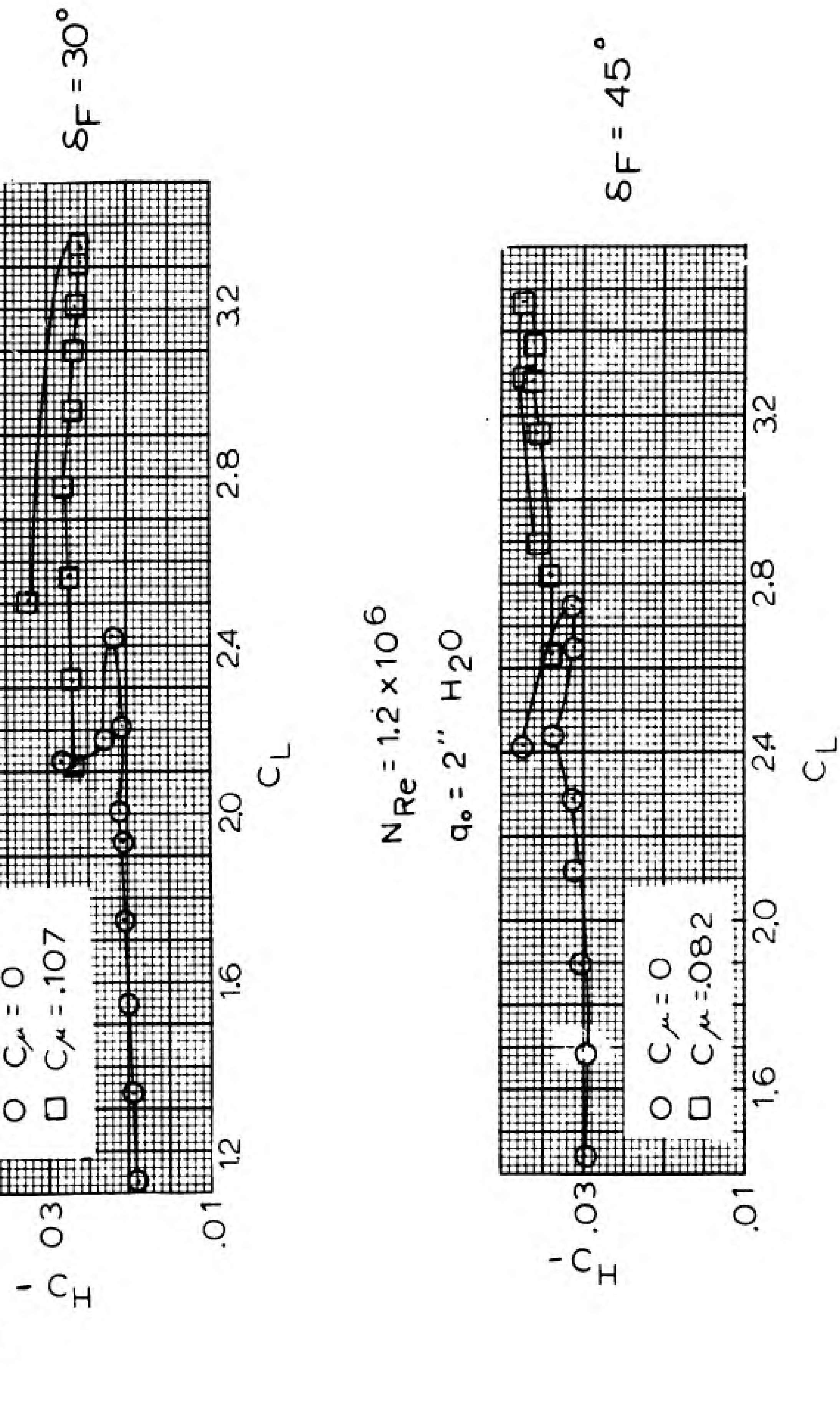

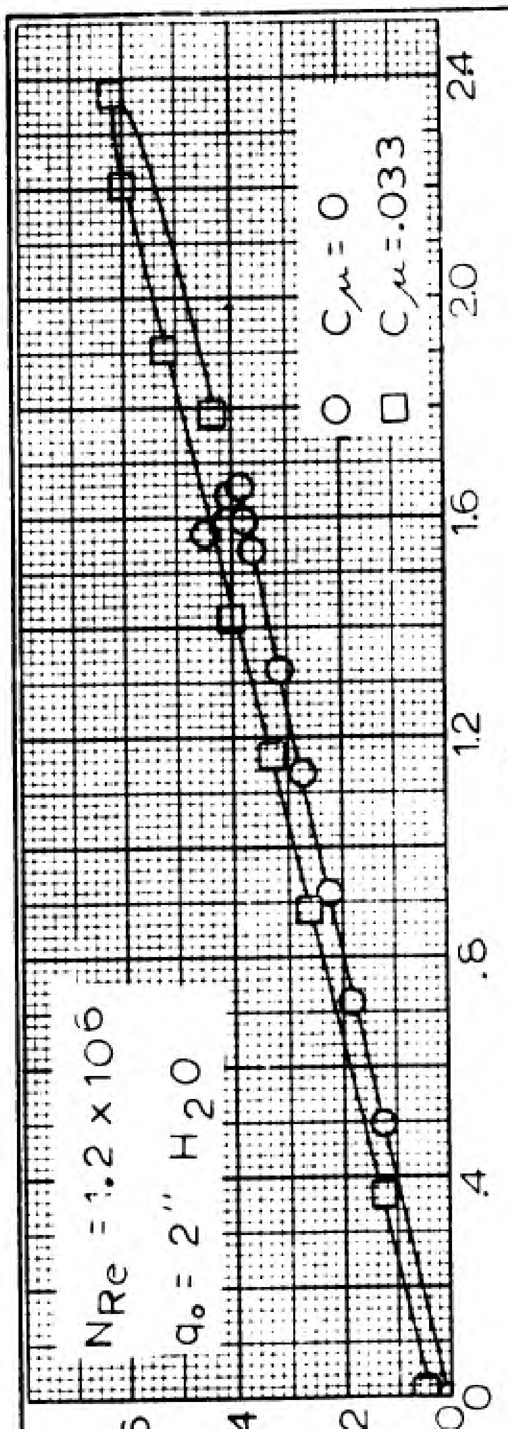

Fig. 30 Effect of Blowing on C_{Mle} ($\delta_F = 0°$)

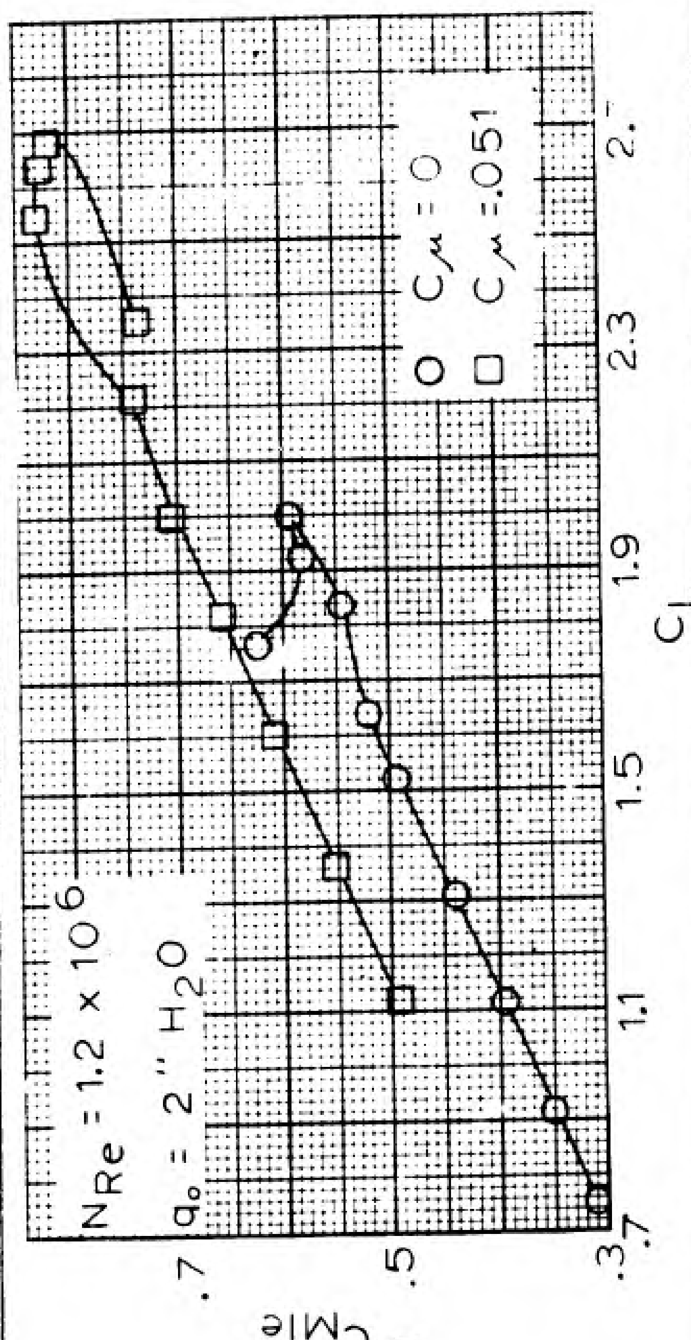

Fig. 31 Effect of Blowing on C_{Mle} ($\delta_F = 15°$)

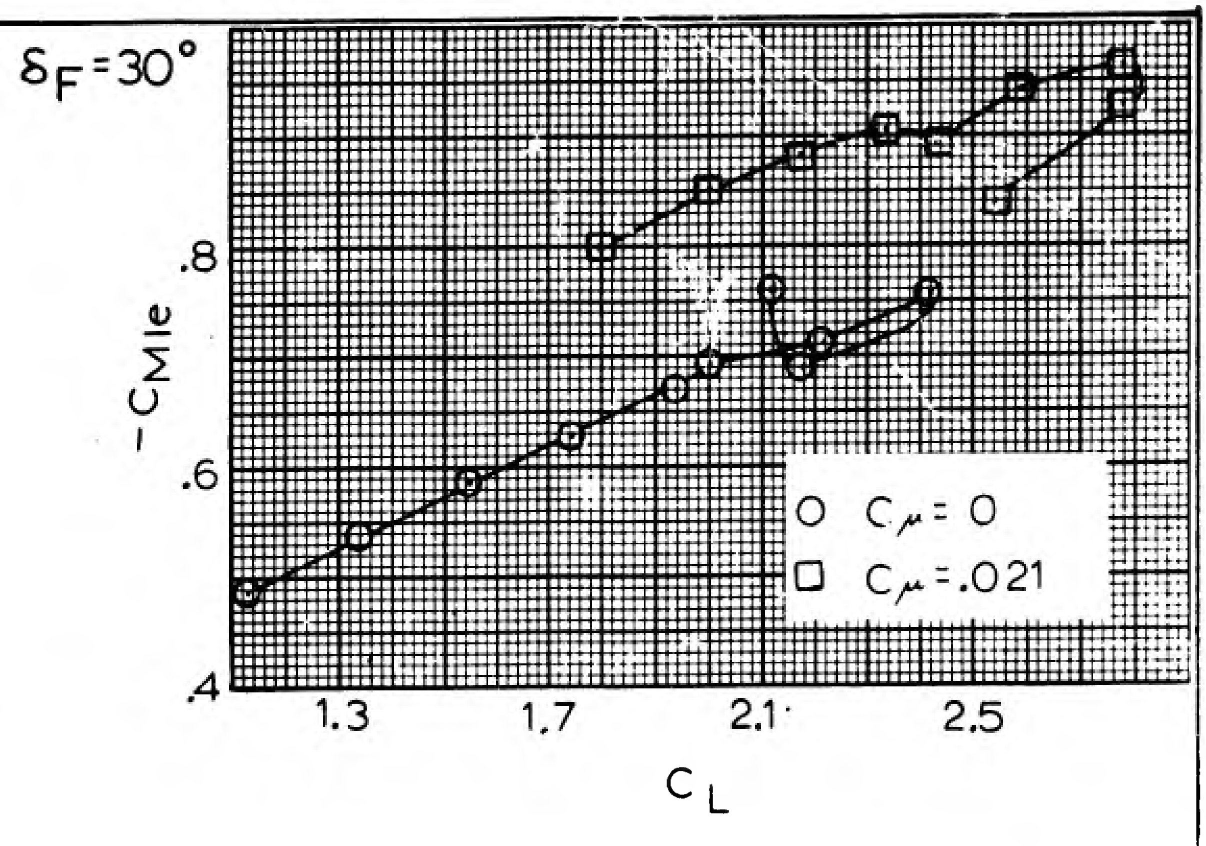

Fig. 32 Effect of Blowing on C_{Mle} ($\delta_F = 30°$ & $45°$)

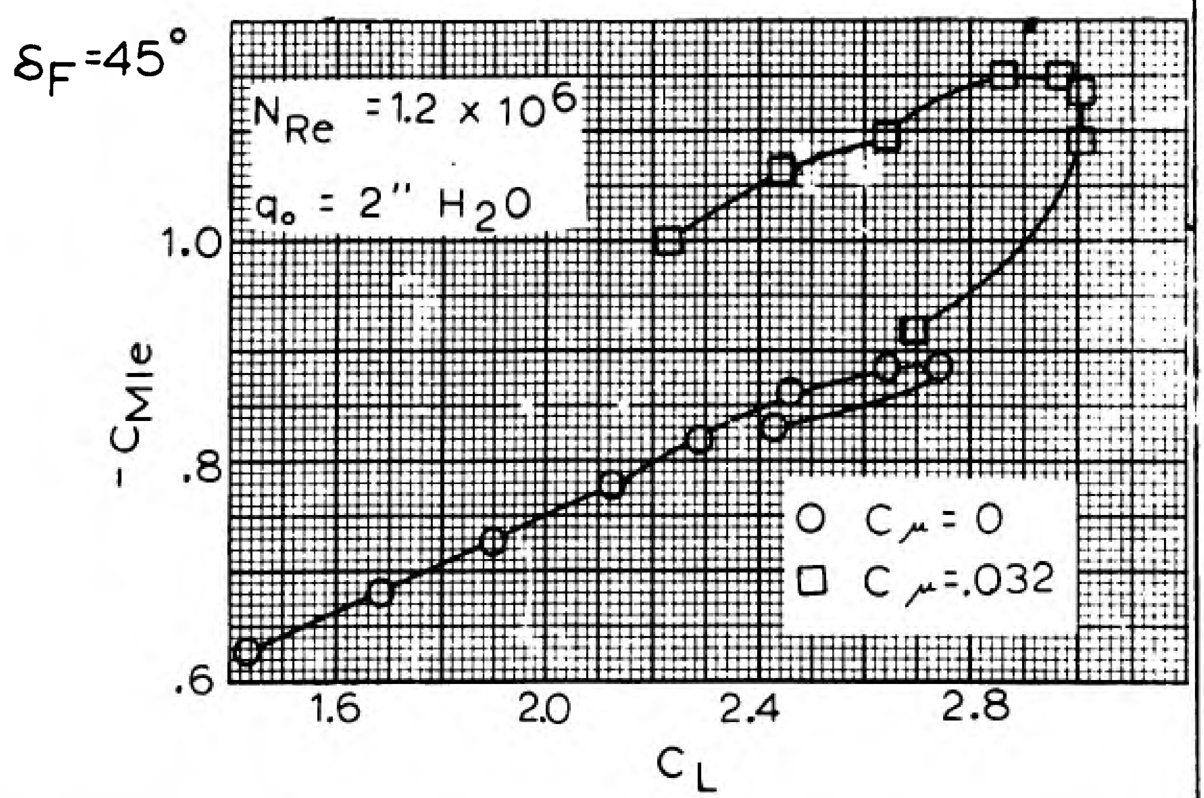

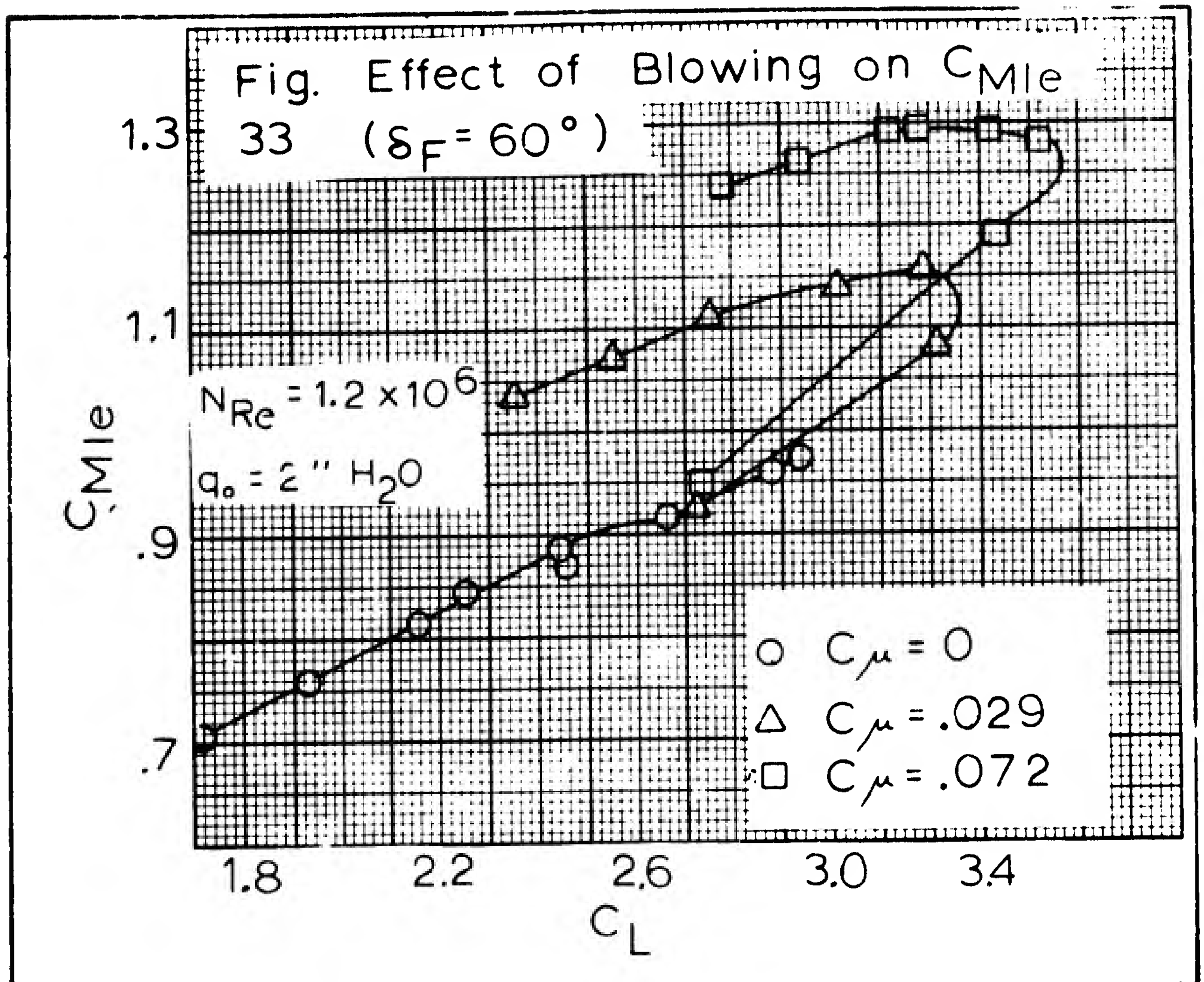
Fig. 33 Effect of Blowing on C_{Mle} ($\delta_F = 60°$)
1.3
1.1
.9
.7
C_{Mle}
$N_{Re} = 1.2 \times 10^6$
$q_o = 2''\ H_2O$
○ $C_\mu = 0$
△ $C_\mu = .029$
□ $C_\mu = .072$
1.8
2.2
2.6
3.0
3.4
C_L

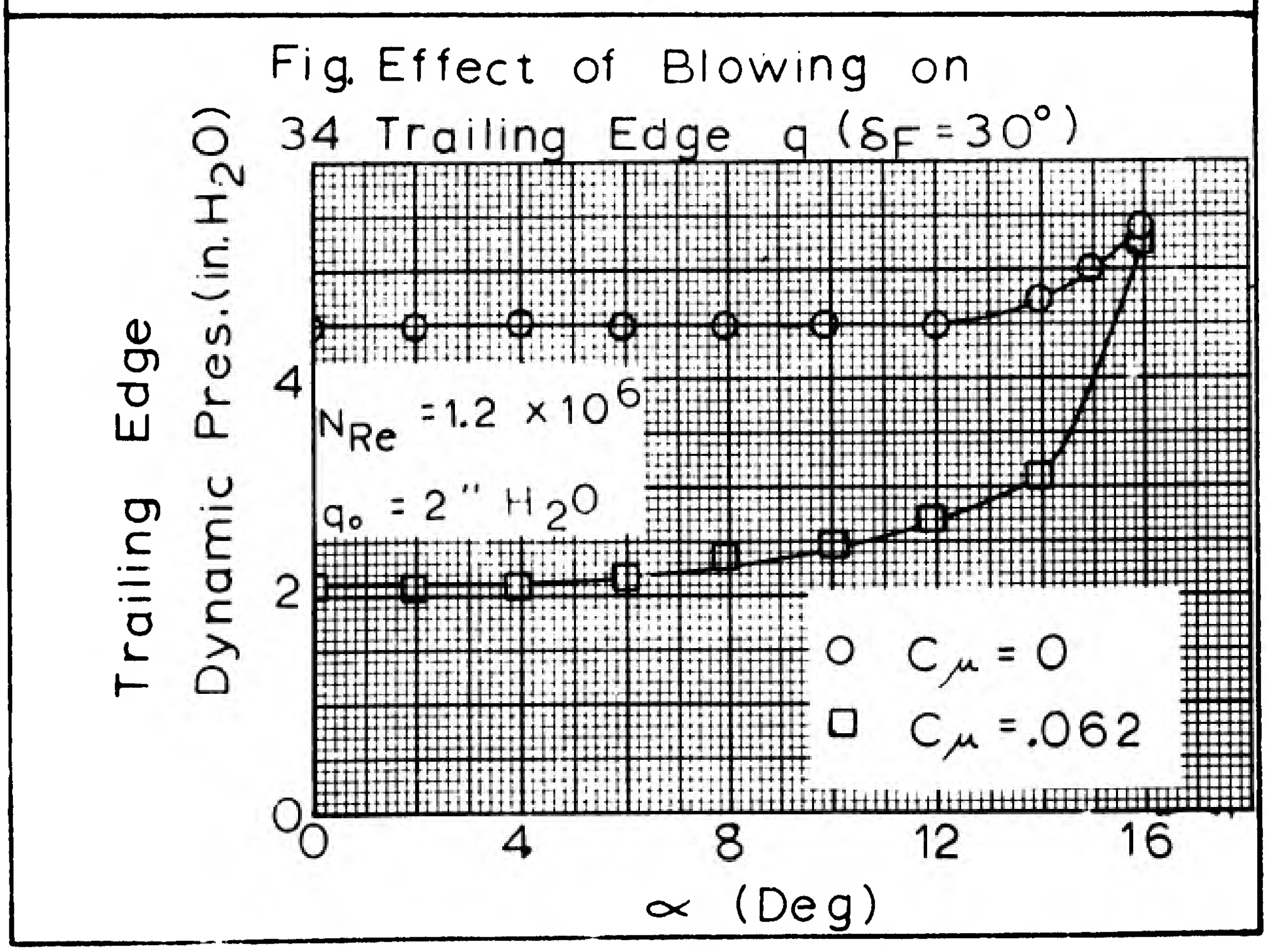
Fig. 34 Effect of Blowing on Trailing Edge q ($\delta_F = 30°$)
Trailing Edge Dynamic Pres. (in. H_2O)
4
2
0
$N_{Re} = 1.2 \times 10^6$
$q_o = 2''\ H_2O$
○ $C_\mu = 0$
□ $C_\mu = .062$
0
4
8
12
16
α (Deg)

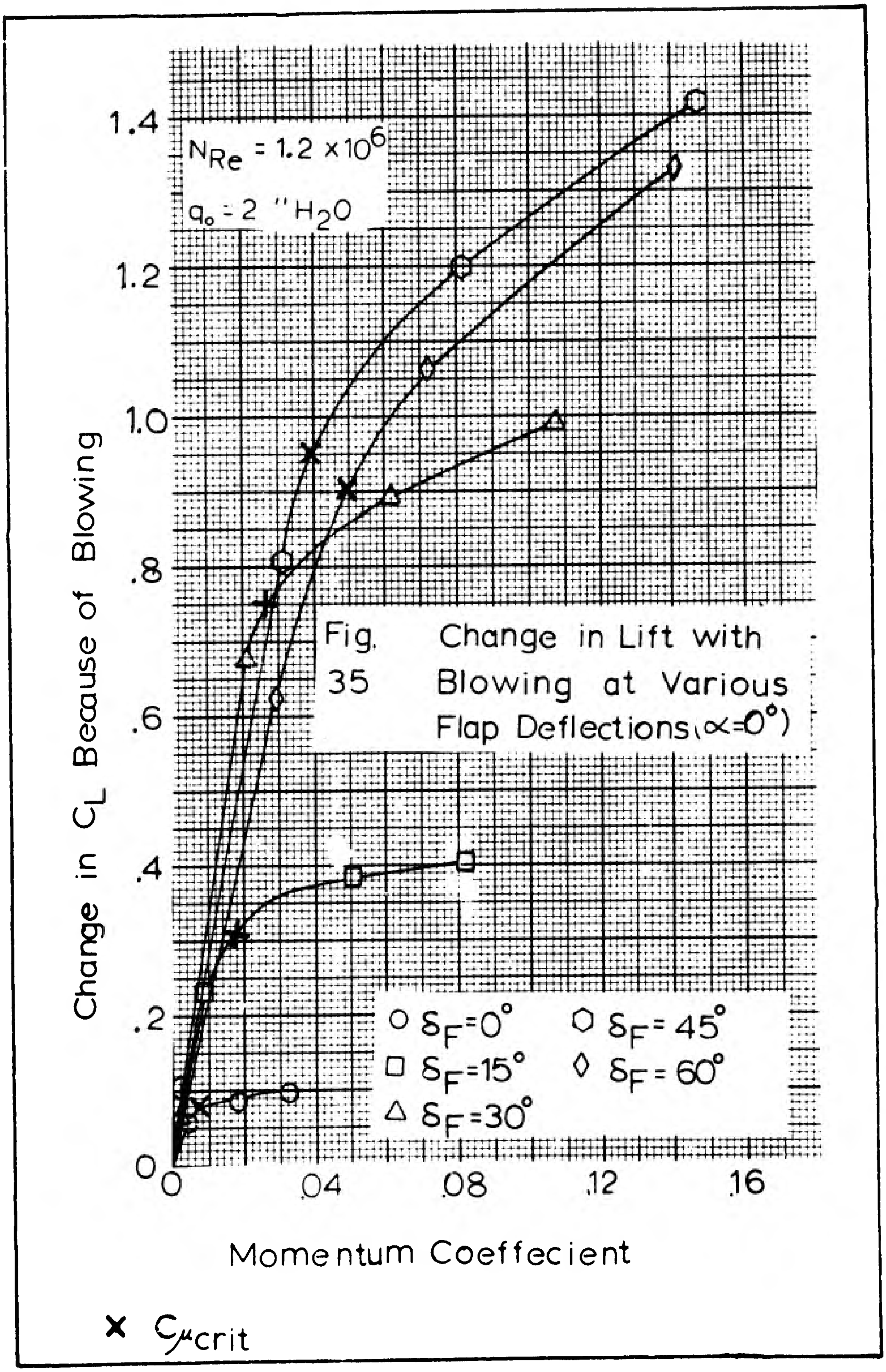

Fig. 35 Change in Lift with Blowing at Various Flap Deflections ($\alpha = 0°$)

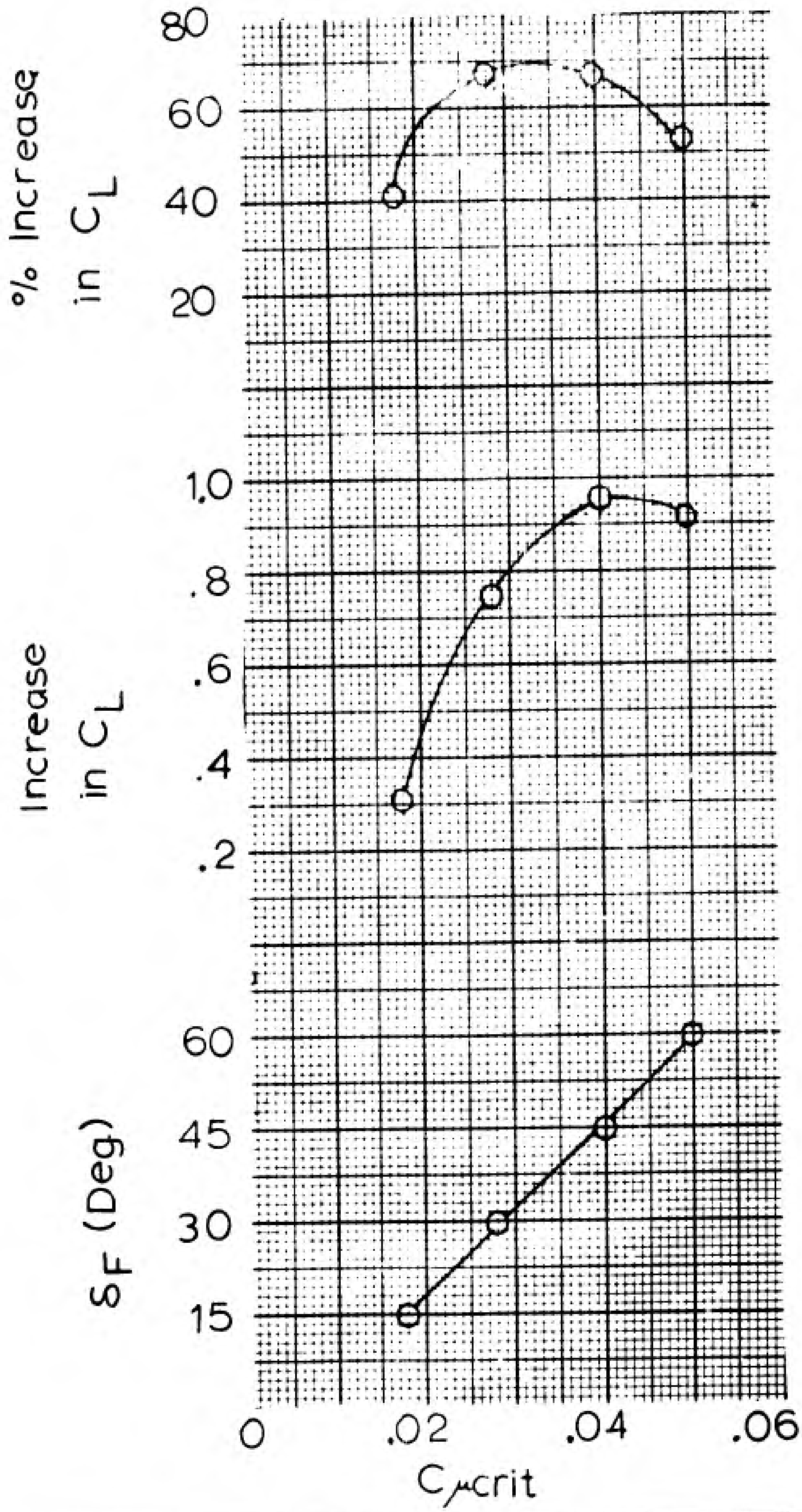

Fig. 36 Variation of C_L & δ_F with $C_{\mu crit}$

$N_{Re} = 1.2 \times 10^6$

$q_o = 2'' \; H_2O$

Appendix B

Data Reduction Computer Program

Explanation

The computer program for the data reduction of the airfoil is a typical Fortran program written for the use in the IBM 1620 or similar computer. The language used in the program is Fortran and was written especially for use with the AFIT Fortran processor.

The computer program received the input data, geometrical, free-stream, and airfoil pressure, and began computation. The first step was the re-numbering of the airfoil pressure data for ease of integration. Next the horizontal and vertical distances from the leading edge to every pressure tap on the airfoil calculated. Using the pressure data and the various distances, the computer then integrated the data numerically, using the Trapezoidal Rule. Then the resulting sectional characteristics were corrected for blocking and the final results were output on punch cards.

Operating Instructions

Input Data Format and Order

The input data consists of the physical location of each pressure tap, tunnel and blowing parameters, and pressure readings over the flap. After loading the object deck and required subroutines (standard loading procedure) the input data can be loaded. The format of the input data and the order of loading are as follows.

Card No. 1 -- Card No. 31. Each card in this range will have two pieces of data punched on it. The first is the distance from the

Leading edge to each pair of pressure taps (taps are located symmetrically over airfoil, except the six on the leading edge of flap) and the second is half the thickness at that point. (All measurements here are fractions of chord.) Table I gives the necessary data.

Card No. 32. This card contains four pieces of data; momentum coefficient, tunnel dynamic pressure, tunnel static pressure, and the average total pressure of the wake. All the pressures are read directly from the appropriate manometers and are relative to the tunnel total head. In other words, the pressures are not absolute and are as read from the manometer boards. One note here, the dynamic pressure has the same magnitude but opposite sign as the static pressure because or the hook-up and the method of calculation. The dynamic pressure and static pressure are read from the airfoil manometer board and the total head of the wake is the average reading of the total head tubes on the rake manometers (outside the "hump").

Card No. 33. This card contains the angle of attack of the model in degrees, the flap deflection in degrees, P_1, P_2, P_3, P_4, P_5, and P_6 from the manometer.

Card No. 34 -- Card No. 39. These cards contain, in order, P_7 through P_{66}, with ten pressure readings per card. Values must be entered for each pressure tap although, for example, at a flap deflection of zero degrees the six taps on the leading edge of the flap will not be exposed to the freestream and their readings are not used in the calculation. A value of zero may be used for these values. Also at 15° flap deflection, there are five zero readings, at 30° there are three zero readings, at 45° there are two zero readings and at 60° there are no zero readings and all taps are exposed to the free stream.

At this point the computer, according to the setting of the Sense Switches, will do one of two things. One, it will calculate all the airfoil sectional characteristics, output the results and look for more airfoil pressure data. (After once feeding in the geometric data, and tunnel and blowing parameters, airfoil pressure data can be fed in until there is a change in either the tunnel parameters, i.e., change in speed, or a change in blowing.) Two, it will read the rake data and calculate the profile drag from the rake pressure readings in addition to the calculations above. If the profile drag is desired, the next paragraphs give the form of the rake data. If only the airfoil calculations are to be performed, set the sense switches according to the next section and keep inputing the airfoil data.

Input Data of Rake Pressure Only

Card No. 40. The data on this card will be four of the static pressure reading in the wake (there are six in all), the manometer tube number, where the drag "hump" begins and the tube number where the "hump" ends. For example, the static pressure reachings might be 6.8, 7.2, 6.8, and 7.0, and the "hump" begins at tube number 37 and ends at tube number 72. The entries on Card No. 40 will be 6.8 7.2 6.8 7.0 37 72.

Card No. 41 -- As Required. In this range as many data points as will fit on a card can be punched on a card. The data entries will be the rake pressure readings beginning with the first reading in the "hump" and proceeding up through the last reading in the "hump". For example, in the example in the above paragraph the pressures range from P_{37} up through P_{72}. If there are static pressure tubes in the "hump", compute the average of the total head tubes on either side and input this reading instead of the static pressure reading.

After all these data have been input to the computer, the computer will output the results on cards and will begin searching for more airfoil pressure data, then rake data, more airfoil pressure data, more rake data, etc. If the tunnel or blowing parameters have changed, use a normal computer reset procedure and re-load the geometric data, the new tunnel and/or blowing data, the airfoil pressure data, and rake data (if required).

Sense Switch Settings

The setting of the sense switches determine what route the computer will take as it proceeds through the program. The program is written so that it may be used in two different procedures. The first is the reduction of the airfoil pressure data only, and the second is the reduction of airfoil pressure data and rake pressure data in one process. Below is listed the different processes and the necessary sense switch settings.

There are also provisions in the program for the pressure coefficient output for each tap, as well as the location of the tap relative to the leading edge. The choices available for this output are controlled by sense switches and are: output of pressure and related data for every computation, which takes a large number of output cards, output of this data for representative computations ($S_F = 0°$, $\alpha = 0°$ and $12°$; $S_F = 30°$, $\alpha = 0°$ and $12°$), which should be sufficient unless other pressure coefficient data are required, and output of no pressure-coefficient data at all. The settings of the sense switches for each of the choices are given below. These settings are applicable for either route taken, i.e., reduction of airfoil data only or airfoil and rake data reduction.

Choice No. 1. Pressure coefficient and related data are output for every run. Sense Switch No. 3 must be OFF and Sense Switch No. 1 must be ON.

Choice No. 2. Pressure coefficient and related data are out for representative runs. Sense Switch No. 3 must be OFF and Sense Switch No. 1 must be ON.

Choice No. 3. No pressure coefficient and related data are output. Sense Switch No. 3 must be ON and Sense Switch No. 1 must be ON.

After choosing the type pressure coefficient output, the next step is the choice of airfoil data reduction only or airfoil and rake data reduction. If reduction of airfoil data only is required, Sense Switch No. 2 must be OFF, but if airfoil and rake data are to be input and reduced, Sense Switch No. 2 must be ON.

Data Reduction Computer Program

```
      DIMENSION P(100),X(67),Y(100),T(31),XX(31)
      DO 1 I=1,31
 1    READ,XX(I),T(I)
      READ,CMU,Q,PSTAT,PORK
 2    READ,AD,AFD,P(1),P(2),P(66),P(3),P(65),P(4)
      READ,P(64),P(5),P(63),P(6),P(62),P(7),P(61),P(8),P(60),P(9)
      READ,P(59),P(10),P(58),P(11),P(57),P(12),P(56),P(13),P(55),P(14)
      READ,P(54),P(15),P(53),P(16),P(52),P(17),P(51),P(18),P(50),P(19)
      READ,P(49),P(20),P(48),P(21),P(47),P(22),P(46),P(23),P(45),P(30)
      READ,P(24),P(25),P(26),P(27),P(28),P(29),P(44),P(31),P(43),P(32)
      READ,P(42),P(33),P(41),P(34),P(40),P(35),P(39),P(36),P(38),P(37)
      A=AD*.0174538
      AF=AFD*.0174538
      X(1) = 0.
      Y(1)=0.
      CA=COS(A)
      SA=SIN(A)
      PUNCH 15
 15   FORMAT(////10X,42HTHE RESULTS OF A SINGLE RUN ARE AS FOLLOWS//)
      PUNCH 80,CMU,AD,AFD
 80   FORMAT(6HCMU = F5.2,9H ALPHA = F5.1,9H DALTA = F5.1//)
      DO 20 I=2,23
      J=68-I
      DA = XX(I)
      DB = T(I)
      X(I) = DA*CA+DB*SA
      Y(I) = DA*SA-DB*CA
      X(J) = DA*CA-DB*SA
 20   Y(J) = DA*SA+DB*CA
      DO 21 I=1,66
 21   P(I)=(P(I)-PSTAT)/Q
      CHI=A+AF
      CHA=COS(CHI)
      SHA=SIN(CHI)
      DO 28 I = 30,36
      J=74-I
      K = I - 6
      DA = XX(K)
      DB = T(K)
      X(I)= (DA-.75)*CHA+DB*SHA+.75*CA
      Y(I) = (DA-.75)*SHA-DB*CHA+.75*SA
      X(J) = X(I) - 2.*DB*SHA
 28   Y(J) = Y(I) + 2.* DB * CHA
      DO 23 K=1,6
      I=23+K
      B = K
      PSI=A+AF+.349076+.174538*B
      X(I)=.75*CA-.039504*COS(PSI)
 23   Y(I)=.75*SA-.039504*SIN(PSI)
      X(37)=.25*CHA+.75*CA
      Y(37)=.25*SHA+.75*SA
```

```
     IF ( SENSE SWITCH 3) 71,43
 71  IF (SENSE SWITCH 1) 41,42
 42  IF(AFD*AFD-30.*AFD)43,70,43
 70  IF (AD*AD-12.*AD) 43,41,43
 41  PUNCH 44
 44  FORMAT(3X,7HSTATION,6X,1HX,12X,1HY,12X,2HCP)
     DO 25 I=1,66
 25  PUNCH 46,I,X(I),Y(I),P(I)
 46  FORMAT(5X,I3,4X,F8.5,6X,F8.6,F8.4)
 43  CL = 0.
     CDP=0.
     W=0.
     CDT=0.
     DO 300 I=1,22
     M=I+1
     DA = X(I)
     DB = Y(I)
     DC = X(M)
     DD = Y(M)
     BC = P(I) + P(M)
     CL = CL +BC*(DC-DA)*.5
     CDP = CDP + BC*(DD-DB)*.5
300  W=W+BC*(DC**2+DD**2-DA**2-DB**2)*.25
     B=AFD*.1
     N=B
     L=30-N
     P(67)=P(1)
     X(67)=0.
     Y(67) = 0.
     DO 105 I = L,66
     M=I+1
     DA = X(I)
     DB = Y(I)
     DC = X(M)
     DD = Y(M)
     BC = P(M)+ P(I)
     CL = CL + BC*(BC-DA)*.5
     CDP = CDP + BC*( DD-DB)*.5
105  W=W+BC*(DC**2+DD**2-DA**2-DB**2)*.25
     CL=CL+(P(L)+P(23))*(X(L)-X(23))*.5
     CDP=CDP+(P(L)+P(23))*(Y(L)-Y(23))*.5
     W=W+(P(L)+P(23))*(X(L)**2+Y(L)**2-X(23)**2-Y(23)**2)*.25
     CH=0.
     DO 110 I=30,43
     M=I+1
     BC = (P(M) + P(I))*.5
     DA = X(M) -X(I)
     DB = Y(M) - Y(I)
     DC = (X(M) + X(I))*.5
     DD = (Y(M)+Y(I))*.5
110  CH =CH+BC*(DA*(DC-.75*CA)+DB*(DD-.75*SA))
110  CH=CH+(P(M)+P(I))*(X(M)-X(I))*((X(M)-X(I))*.5-.75*CA)*.5
     CL = -1.* CL
```

```
      CDP = - 1. * CDP
 55   IF (SENSE SWITCH 2) 22,63
 22   Y(1) = .5
      Y(2)=1.
      Y(3)=3.
      Y(4)=6.
      Y(5)=9.
      Y(6)=12.
      Y(7)=15.
      Y(8)=21.5
      F=31.75
      DO 99 I=9,93
      Y(I)=F
 99   F=F+.25
      Y(94)=Y(93)+1.1875
      Y(95)=Y(94)+3.
      Y(96)=Y(95)+3.
      Y(97)=Y(96)+3.
      Y(98)=Y(97)+3.
      Y(99)=Y(98)+2.
      Y(100)=Y(99)+.5
      READ,P5,P13,P71,P96,JLR,JUR
      PRST = (P5+P13+P71+P96)*.25
      Q0=PRST-PORK
      DO 60 I=JLR,JUR
      READ,PP
      P(I) = PRST - PP
      G=P(I)/Q0
      E=SQRT(G)
      F=E-G
 60   P(I)=F
      JUR=JUR-1
      DO 62 I=JLR,JUR
      J=I+1
 62   CDT=CDT+(P(I)+P(J))*(Y(J)-Y(I))*.5
 63   CDT = CDT/15.
      CDTC=CDT*1.02*(.96835-.1250*CDT)
      ADC=AD+.4685*CL
      AA=.92752-.125*CDT
      CLC=CL*AA
      CDPC=CDP*AA
      CHC=CH*AA
      WC=W*AA
      PUNCH 11
 11   FORMAT(/20X,34HTHE FOLLOWING DATA ARE UNCORRECTED//)
      PUNCH 12
 12   FORMAT(5HALPHA,6H DELTA,9X,2HCL,8X,3HCDP,9X,2HCD,8X,4HCMLE,8X2HCH)
      PUNCH 13,AD,AFD,CL,CDP,CDT,W,CH
 13   FORMAT(//F6.2,1X,F5.1,4X,5F11.8)
      PUNCH 14
 14   FORMAT(//20X,32HTHE FOLLOWING DATA ARE CORRECTED//)
      PUNCH 12
      PUNCH 13,ADC,AFD,CLC,CDPC,CDTC,WC,CHC
      GO TO 2
      END
```

Vita

[redacted]

After completing his work in 1957 at Senatobia High School, Senatobia, Mississippi, he enrolled at Mississippi State University, Starkville, Mississippi. In May 1961 he received his Bachelor of Science in Aeronautical Engineering and his commission as a Second Lieutenant in the United States Air Force. He entered active duty in September 1961 and served as an Aircraft Maintenance Officer until enrollment at the Air Force Institute of Technology.

[redacted]

This thesis was typed by Mrs. Imogene J. Hoffer.